UNIVERSITÀ DEGLI STUDI DI PADOVA

Corso di Laurea Magistrale in Medicina e Chirurgia

Dipartimento di Medicina - DIMED

Direttore: Ch.mo Prof. Roberto Vettor

U.O.C. Istituto di Radiologia

Direttore: Ch.mo. Prof. Emilio Quaia

TESI DI LAUREA

MYOCARDIAL T1 MAPPING BY A QUANTITATIVE SEGMENTAL APPROACH: NORMAL VALUES, EFFECTS OF AGING, AND GENDER DIFFERENCES

Relatrice: Prof.ssa Alessia Pepe

Correlatrice: Dott.ssa Amalia Lupi

Laureanda: Eleonora Dal Pos

Anno Accademico 2021-2022

ABSTRACT (ENG)

Background In the context of Cardiac Magnetic Resonance (CMR), modern-day T1 mapping technique allows for precise and quantitative characterization of the myocardial tissue, and it is significantly changing the clinical management in the patients with cardiac involvement. It can be used as a diagnostic tool in various pathological heart conditions such as fibrosis, iron overload or amyloid infiltration significantly reducing the necessity of biopic exams. The major limit in spreading these techniques in clinical and research setting is the strong dependence to the scanner and sequence used. Thus, each center should obtain their own set of reference values for T1 mapping by studying a population of healthy subjects. To the best of our knowledge, this is the first study that evaluate 16 segmental and global T1 normal values with a 1.5 T Siemens scanner, using MOLLI sequences analysed with cvi42 software in a large study population stratified for sex and age.

Objectives The aim of the study was to prospectively assess a population of healthy volunteers, using quantitative T1 mapping technique by a Siemens, MAGNETOM Avanto Fit 1.5 T scanner to obtain segmental and global T1 values of the myocardium and to evaluate the association between them and physiological variables of the included subjects. Then, we applied the reference values obtained in our Institute, compared to literature values, in same illustrative cases for testing the clinical value of sex and age specific normal cut off values for classifying health versus disease.

Materials and methods Fifty healthy volunteers aged between 20 and 69 years, male-to-female ratio 1:1, underwent CMR without contrast agent. They had no cardiovascular risk factors, no history of cardiovascular and systemic diseases, and a negative EKG. Basal, mid, and distal short axis slices were obtained with Modified Look Locker Inversion Recovery (MOLLI) sequences for the T1 quantification. The images obtained were analysed using a commercially available software (cvi42) to evaluate T1 values in all 16 left ventricular AHA segments; the global T1 values were the averages of the single segments' values.

The statistical analysis of the data obtained was then carried out to determine the presence of any association between T1 values and age, gender, myocardial wall

thickness, and cardiac cycle phases. A p-value < 0.05 was considered statistically significant. To verify the normal distribution of the parameter, Shapiro-Wilk test was performed. To assess the correlation between variables, Pearson's or Spearman's correlation index were used. The comparison between two groups was carried out with the t-test for independent samples or the Mann-Whitney test. To examine regional differences of the T1 values, the ANOVA method or Kruskal-Wallis test were used; Bonferroni's correction was applied in all comparisons between multiple factors.

A subset of subjects, representative of the study population, was selected to repeat the CMR protocol at one-hour intervals and assess inter-study reproducibility; intra-operator and inter-operator reproducibility were also assessed on these patients to confirm the stability of the acquired data. These reproducibility studies included the definition of the Bland-Altman limits for the difference of the average values and of the ICC of the various datasets.

Bland-Altman limits and ICC were applied to all healthy volunteers to study T1 differences between systole and diastole.

Results Fifty-three healthy volunteers were prospectively enrolled to perform a CMR; among these, three were excluded from the analysis due to pathological cardiac findings. The subjects included in this study were 25 males and 25 females between 20 and 69 years of age, 5 per decade of age (mean age 43.2 ± 13.9). In all patients, the examination was successfully completed.

The global T1 value in all subjects averaged at 993.2 ± 24.0 (range 945.2-1041.2 ms); the lowest average T1 value was in the middle anterior segment (978.4 ms), while the highest one was in the basal inferior segment (1010.9 ms). Globally, there was no significant difference between the sections considering all subjects: basal vs mid-ventricular p=0.4, mid-ventricular vs apical p=0.8, basal vs apical p=0.8; in males only, basal vs mid-ventricular section values showed a significant difference (p=0.01). Significantly lower mean T1 values were found in males at mid and apical levels (p=0.001 and p=0.009, respectively).

The overall measured T1 values were lower in male than in female subjects (983.8 ± 20.5 vs 1002.5 ± 23.9; p= 0.004). A weak positive correlation was found with age (p=0.05).

Greater wall thickness was found in male subjects (p<0.001 in all considered segments), but no statistically significant correlation between wall thickness and T1 values, neither globally nor segmentally.

The analyses concerning changes in T1 related to cardiac cycle phases showed a statistically significant difference (p=0.038).

The reproducibility analyses showed good correlations between the various datasets (ICC>0.80 in all cases).

Conclusions MOLLI sequences allow for a robust and reproducible quantification of segmental and global myocardial T1 values. In our study, the different values obtained during different acquisition phases suggest for implementing specific reference values, in order to avoid systematic errors in the identification of pathological findings. The obtained age- and gender-specific segmental values can be used by the Institute of Radiology in the University of Padua and probably in any center that utilizes the same sequences and scanner. By this way it is possible to optimize the quantitative T1 mapping technique for accurate characterization of the myocardium by MRI.

ABSTRACT (IT)

Background Nel contesto della risonanza magnetica cardiaca (RMC), la nuova tecnica di mapping T1 consente una caratterizzazione precisa e quantitativa del tessuto miocardico e sta cambiando significativamente la gestione clinica dei pazienti con coinvolgimento cardiaco. Questa può essere utilizzata come strumento diagnostico in varie condizioni patologiche cardiache, quali fibrosi, sovraccarico di ferro o infiltrazione di amiloide, riducendo significativamente la necessità di ricorrere ad esami bioptici. Il limite maggiore nella diffusione di questa tecnica in ambito clinico e di ricerca è la forte dipendenza dalla singola apparecchiatura e dalla tipologia di sequenza utilizzata. Pertanto, ogni centro dovrebbe ottenere il proprio set di valori di riferimento per il mapping studiando una popolazione di soggetti sani. Al meglio delle nostre conoscenze, questo è il primo studio che valuta in un'ampia popolazione, stratificata per sesso ed età, i valori normali di T1 a 16 segmenti e globale, utilizzando uno scanner Siemens 1.5 T e sequenze MOLLI analizzate con il software cvi42.

Scopo dello studio Lo scopo dello studio è stato quello di valutare prospetticamente una popolazione di volontari sani, utilizzando la tecnica quantitativa di T1 mapping con uno scanner Siemens, MAGNETOM Avanto Fit 1,5 T, al fine di ottenere valori segmentali e globali di T1 del miocardio e valutare l'associazione tra questi e le variabili fisiologiche dei soggetti reclutati. Quindi, abbiamo applicato, i valori di normalità ottenuti per il nostro Istituto, rispetto a quelli della letteratura, in alcuni casi esemplificativi per testare il valore clinico dei cut-off di normalità specifici per sesso ed età nel classificare normali e patologici.

Materiali e metodi Sono stati sottoposti a RMC senza mezzo di contrasto cinquanta volontari sani di età compresa tra i 20 ed i 69 anni, con un rapporto M: F pari a 1:1. Essi non presentavano fattori di rischio cardiovascolare, né anamnesi di malattie cardiovascolari e sistemiche, e avevano un ECG negativo. Immagini delle sezioni in asse corto basali, medie e distali sono state acquisite mediante sequenze Modified Look Locker Inversion Recovery (MOLLI) per la quantificazione dei valori di T1. Le immagini ottenute sono state analizzate con un software commercialmente disponibile (cvi42) per valutare i valori di T1 in tutti i 16

segmenti del ventricolo sinistro, secondo la classificazione AHA; i valori globali di T1 sono stati ricavati dalle medie dei valori dei singoli segmenti.

L'analisi statistica dei dati ottenuti è stata quindi effettuata per determinare la presenza di eventuali associazioni tra i valori di T1 ed età, sesso, spessore della parete miocardica (per i segmenti del ventricolo medio, in cui è stata effettuata la misurazione) e fasi del ciclo cardiaco. Un valore $p < 0,05$ è stato considerato statisticamente significativo. Per verificare la distribuzione normale dei parametri, è stato eseguito il test di Shapiro-Wilk. Per valutare la correlazione tra le variabili, sono stati utilizzati l'indice di correlazione di Pearson o di Spearman. Il confronto tra due gruppi è stato effettuato con il test t per campioni indipendenti o il test di Mann-Whitney. Per esaminare le differenze regionali dei valori di T1, sono stati utilizzati il metodo ANOVA o il test di Kruskal-Wallis; la correzione di Bonferroni è stata applicata in tutte le comparazioni tra fattori multipli.

Una sottopopolazione di soggetti, rappresentativa della popolazione in studio, è stata selezionato per ripetere il protocollo RMC a distanza di un'ora e valutare la riproducibilità inter-studio; su questi pazienti è stata valutata anche la riproducibilità intra-operatore e inter-operatore per confermare la stabilità dei dati acquisiti. Gli studi di riproducibilità hanno incluso la definizione dei limiti di Bland-Altman per la differenza dei valori medi e dell'ICC dei vari set di dati.

I limiti di Bland-Altman e l'ICC sono stati applicati a tutti i volontari sani per studiare le differenze dei valori di T1 tra sistole e diastole.

Risultati Cinquantatré volontari sani sono stati arruolati prospetticamente per eseguire una RMC; tra questi, tre sono stati esclusi dall'analisi a causa del riscontro di reperti patologici a livello cardiaco. I soggetti inclusi nel presente studio sono 25 maschi e 25 femmine di età compresa tra 20 e 69 anni, 5 per decade di età (età media 43,2 ± 13,9). In tutti i pazienti l'esame è stato completato con successo.

Il valore T1 globale in tutti i soggetti è risultato essere in media 993,2 ± 24,0 (range 945,2-1041,2 ms); il valore T1 medio più basso era nel segmento anteriore medio (978,4 ms), mentre quello più alto era nel segmento inferiore basale (1010,9 ms). Globalmente, non è stata rilevata alcuna differenza significativa tra le sezioni

considerando tutti i soggetti: basale vs medio-ventricolare p=0,4, medio-ventricolare vs apicale p=0,8, basale vs apicale p=0,8; considerando solo i maschi, i valori della sezione basale vs medio-ventricolare hanno mostrato una differenza significativa (p=0,01). Inoltre, sono stati riscontrati valori medi di T1 significativamente più bassi nei maschi a livello medio e apicale (p=0,001 e p=0,009, rispettivamente) rispetto alle femmine.

I valori globali di T1 misurati nei soggetti di sesso maschile sono risultati inferiori rispetto a quelli di sesso femminile (983,8 ± 20,5 vs 1002,5 ± 23,9; p= 0,004). È stata riscontrata una debole correlazione positiva con l'età (p=0,05).

Nei soggetti di sesso maschile è stato riscontrato un maggiore spessore della parete (p<0,001 in tutti i segmenti considerati), ma non è stata riscontrata alcuna correlazione statisticamente significativa tra lo spessore della parete e i valori di T1, né a livello globale né a livello segmentario.

Le analisi relative alle variazioni di T1 in relazione alle fasi del ciclo cardiaco hanno mostrato una differenza statisticamente significativa (p=0,038).

Le analisi di riproducibilità hanno mostrato buone correlazioni tra i vari dataset (ICC>0,80 in tutti i casi).

Conclusioni Le sequenze MOLLI consentono una quantificazione robusta e riproducibile dei valori T1 segmentali e globali del miocardio. Nel nostro studio, i diversi valori ottenuti durante le varie fasi di acquisizione suggeriscono l'implementazione di valori di riferimento specifici, al fine di evitare errori sistematici nell'identificazione di reperti patologici. I valori segmentali ottenuti, specifici per età e sesso, possono essere utilizzati dall'Istituto di Radiologia dell'Università di Padova e realisticamente in qualsiasi centro che utilizzi le stesse sequenze e lo stesso scanner. In questo modo è possibile ottimizzare la tecnica di mappatura T1 quantitativa per un'accurata caratterizzazione tissutale del miocardio mediante RM.

BACKGROUND

1. INTRODUCTION TO MYOCARDIAL MAPPING

Cardiac magnetic resonance (CMR) represents to date the 'gold standard' radiological method for non-invasive tissue characterisation of the myocardium. CMR outweighs all the other cardiac imaging methods (such as echocardiography, nuclear imaging and MDCT) because of its multiparametric capabilities that allow a comprehensive cardiac examination. (Karamitsos et al., 2020) Since its first applications in the cardiovascular field at the end of the last century, MRI has recognised its specific diagnostic strength in its ability to characterise myocardial tissue, through non-parametric sequences evaluated qualitatively or semi-quantitatively, for the identification of oedema, fat, fibrosis, iron, or amyloid. The application of these techniques in clinical practice has contributed to a significant improvement in the prognosis of cardiologic patients.

However, conventional nonparametric sequences are strongly dependent on the type of sequence, coil, and scanner manufacturing company used (Kawel-Boehm et al., 2015); other limitations are due to the signal alteration is not always matched with tissue alteration, and the failure to compare data either between different patients or within the same patient effectively over time, given the qualitative and semi-quantitative nature of the technique itself.

In the last decade, the availability, first in research and later clinical settings, of sequences for the quantitative measurement of T1, T2 and T2* (T2 star) relaxation times is representing a revolution in the management of the cardiologic patients.

Through these techniques, it is now possible to observe tissue alterations, such as iron overload (due to hemochromatosis or multiple transfusions), glycosphingolipid overload in Anderson-Fabry disease, myocardial interstitium changes, such as fibrosis or amyloidosis. In addition, it is possible to identify myocardial oedema due to ischemic or non-ischemic genesis. (Messroghli et al., 2017)

In particular, the T1, T2 and T2* mapping techniques allow a quantitative evaluation of the alterations of the signal coming from the myocardium, closely

related to the tissue characteristics of the same, as demonstrated by the correlation studies with the biopsies. This represents a significant step forward in the diagnostic capacity of various myocardial pathologies, which in the past often required, and still require, invasive investigations in order to be correctly diagnosed with a quantitative approach.

The main advantages of a quantitative evaluation are objective differentiation between pathology and normal conditions, grading of disease severity, and the possibility of comparing different groups of patients and normal subjects. (Kawel-Boehm et al., 2015)

Another important aspect of the mapping techniques is that the obtained information has prognostic relevance. It permits pathology detection and quantification, so the development of the disease can be monitored under treatment. Consequently, mapping techniques have the potential to act as biomarkers to help diagnostic decision making in several pathologies(Granitz et al., 2019), leading to a significant improvement in the prognosis of patients with cardiac diseases.

In the early stages, T1, T2, and T2* mapping techniques were applied by considering only the middle interventricular septum of the left ventricle, as it was less prone to artifacts.(Pennell et al., 2013) (Messroghli et al., 2017) Now, however, thanks to technological improvement, it is possible to analyse the entire left ventricular myocardium with a global or segmental approach according to the 16 segments defined by the American Heart Association (AHA) (Cerqueira et al., 2002). The segmental approach has the intrinsic advantage of higher sensitivity diagnosis in the case of non-diffuse tissue changes. (Meloni, et al., 2021)

Parametric mapping techniques promise improvements in the treatment of the cardiology patient through better quantitative diagnostics and inter- and intra-patient comparability, allowing patients to be followed over time, also improving the decision-making process, and consequently treatment.

Furthermore, the use of mapping techniques in the context of medical research allows quantitative endpoints to be set in phase 2 and 3 clinical trials without the need for invasive testing.

The major limitation to the full clinical and research use of myocardial mapping techniques is that they are strongly dependent on the scanner manufacturer, the type of sequence used, and the image acquisition mode. This makes it difficult to compare values between centres. (Messroghli et al., 2017) In addition, there is variability due to gender and age, for which it is necessary to identify normal T1 values in relation to various age groups and specific gender.

1.1 DEFINITIONS

The table below reports the main technical terms referred to in this study [Table I].

Table I: Technical terms of CMR parametric mapping technique (Messroghli et al., 2017).

Term	Meaning
T1 [ms]	Time constant representing the recovery of longitudinal magnetization (spin–lattice relaxation)
Native T1	T1 in the absence of an exogenous contrast agent
T2 [ms]	Time constant representing the decay of transverse magnetization (spin-spin relaxation)
T2* [ms]	Time constant representing the decay of transverse magnetization in the presence of local field inhomogeneities
ECV [%]	Extracellular volume fraction, calculated by $ECV = \frac{\left(\frac{1}{T1myo_{post\,Gd}} - \frac{1}{T1myo_{native}}\right)}{\left(\frac{1}{T1blood_{post\,Gd}} - \frac{1}{T1blood_{native}}\right)} \times (100 - hematocrit)$ where myo = myocardium; blood = intracavitary blood pool; hematocrit = cellular volume fraction of blood [%]
Synthetic ECV [%]	ECV where hematocrit is not measured by laboratory blood sampling but derived from blood T1
Parametric mapping	A process where a secondary image is generated in which each pixel represents a specific magnetic tissue property (T1, T2, or T2*) or a derivative such as ECV) derived from the spatially corresponding voxel of a set of co-registered magnetic resonance source images

1.2 T1 RELAXATION TIME

T1 (spin-lattice) relaxation or longitudinal relaxation is the process by which the magnetization of protons exposed to a radiofrequency pulse regrows along the longitudinal (z) axis until it returns to its initial value at equilibrium.

The recovery of Mz is an exponential process with a time constant T1 [Figure 1]:

$M_z=M_0(1-e^{(-t/T1)})$

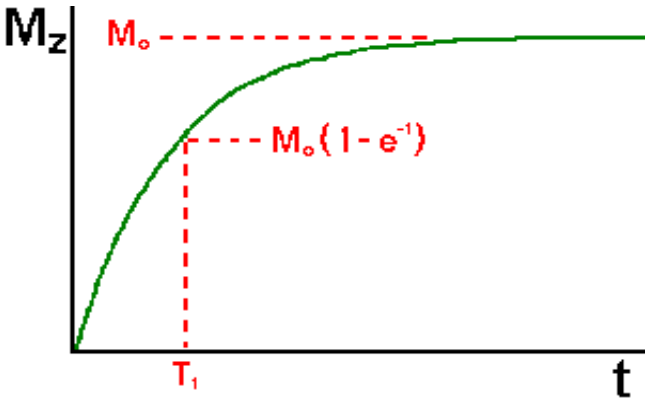

Figure 1: Longitudinal relaxation given by an exponential recovery curve.

T1 therefore represents the time after excitation required to reach a longitudinal magnetization value (M_z) corresponding to 63% (1-1/e) of the starting value (M_0) [Figure 2].

After a time t=T1, the longitudinal magnetization is: $M_Z \approx 0.63 M_0$.

After a time t=5T1, the longitudinal magnetization could be considered $M_z \approx M_0$

The z component first grows rapidly, then more slowly, approaching the initial value. This process is due to the loss of energy given by the previous excitation, released from the high energy state protons returning to the low energy state and transferring it to the surrounding lattice environment, where lattice means everything that is not the spin of hydrogen nuclei. The exact relaxation time T1 depends on the lattice environment of the protons, and so it is dependent on the tissue that has been analysed.

The longitudinal relaxation time T1 is expressed in ms.

Different tissues have different T1 values. Fat has a very short T1 relaxation time, while cerebrospinal fluid (CSF) has a long T1 time. This depends on the number of protons (and therefore spin) in the tissue and on the amount of lattice around it.

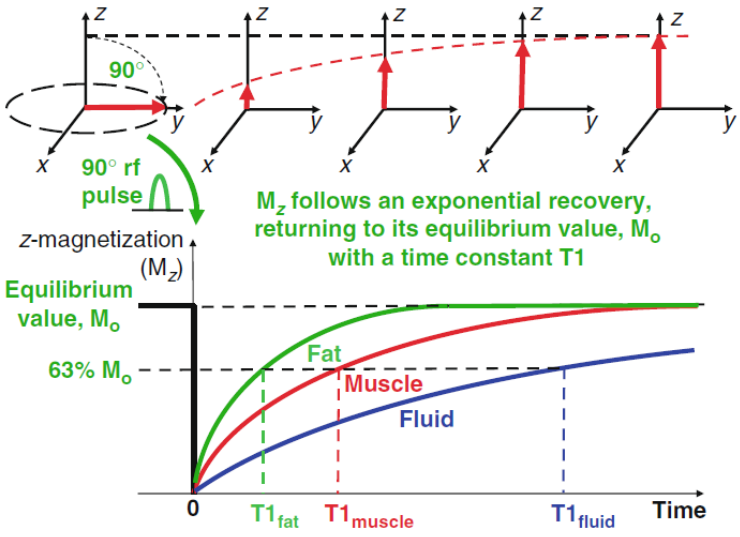

Figure 2: Following a 90° rf pulse, the z component of the net magnetization, Mz is reduced to zero, but then recovers gradually back to its equilibrium value if no further pulses are applied. The recovery of Mz is an exponential process with a time constant T1. This is the time at which the magnetization has recovered to 63% of its original value. (Plein et al., 2011)

T1 relaxation time is lengthened if there is an increased free water content in tissues and is shortened by the presence of iron, fat, or gadolinium-based contrast agents. (Karamitsos et al., 2020)

The T1 relaxation process is much slower than T2 relaxation. These are two independent processes occurring simultaneously, governed by two different mechanisms that both allow energy to be released from the system and return to the basal state.

2. RATIONALE FOR USING PARAMETRIC MAPPING

Through parametric mapping techniques, in contrast to conventional CMR images, it is possible to absolutely quantify changes in the magnetic properties of the myocardium.

Mapping permits both visualisation and quantification of the disease process, so it can be detected whether it is diffuse or focal.(Messroghli et al., 2017)

Conventional MRI techniques require the presence of a reference tissue to detect changes in myocardial tissue composition using reference ROIs (whether in remote myocardium or skeletal muscle). For T1-mapping, this threshold-based post-processing method is not necessary, even though it may be needed when sizing myocardial injury. This makes quantitative techniques such as T1-mapping less prone to subjectivity and error. (Dall'Armellina et al., 2012)

A series of images must be acquired at different echo times (TE) to obtain relaxation time values. The T1, T2 or T2* relaxation time can be then calculated on a pixel-by-pixel basis to obtain a signal decay curve. In order to be accurate and to avoid bias, two conditions must be met:(Messroghli et al., 2017)

1. One must correct according to the variation in weight of other factors, such as different relaxation times or diffusion, if it is not negligible.

2. There must be as little movement as possible between images in the series. Therefore, breathing, and cardiac motion artefacts must be avoided; this is possible by acquisition with cardiac gating and by hold-breath acquisition.

One can also use an algorithm called MOCO (MOtion COrrection), when acquiring single-shot images (using a single RF pulse to acquire the entire K-space) to reduce motion artefacts. Motion correction (MOCO) reduces artefacts due to cardiac motion and shape changes caused by respiration, arrhythmias, or imperfect gating.(Shanbhag et al., 2011)

2.1 T1 MAPPING

T1 mapping is a MR technique useful for calculating the longitudinal relaxation time of specific tissues, such as cardiac tissue. The values obtained can be used to compose a parametric map.

The Modified Look Locker Inversion Recovery (MOLLI) (Messroghli et al., 2004) sequence is one of the most used for myocardial T1 mapping and allows the images acquisition within a single breath-hold.

It is very important to define which sequences and which protocols are being used to perform T1 mapping because even minor changes in protocol parameters can impact T1 values. (Meloni, et al., 2021)

Since T1 relaxation values are influenced by magnetic field strength, equipment, manufacturer, and sequence type, for a correct T1 mapping application, every centre should obtain their own reference T1 values in order to rule out an appropriate interpretation of the acquired T1 maps.(Demirkiran et al., 2019) (Messrogli, 2017

Native T1 maps are made of a parametric colour encoded anatomical map in which the T1 value is encoded in each pixel.(Carrick et al., 2016)

It requires the acquisition of multiple images to derive the T1 recovery curve, allowing to build a pixelwise illustration of an absolute T1 relaxation time through the generation also of a colour-encoded map to simplify visual interpretation [Figure 3].

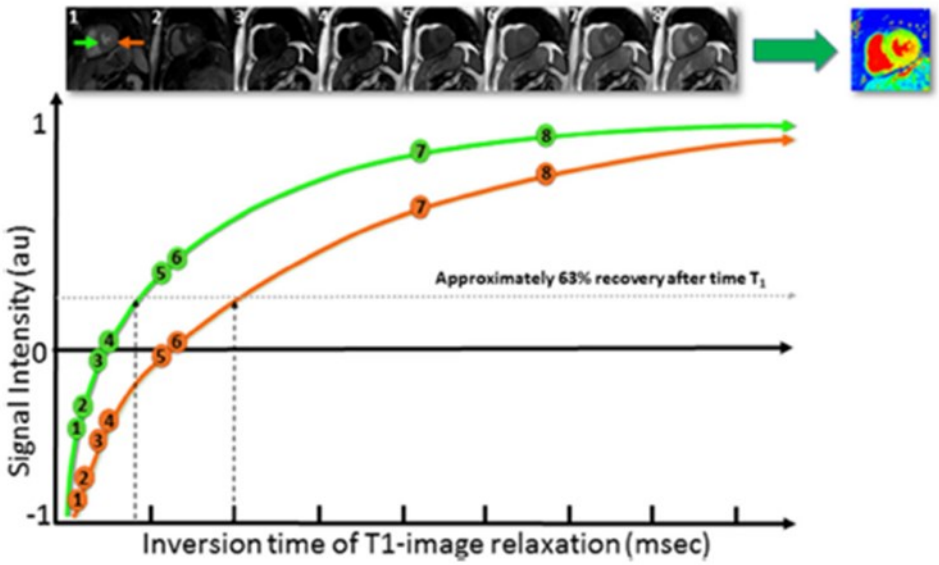

Figure 3: T1 map generation. For illustrative purpose, the orange arrow and relaxation curve refer to an area of myocardial infarction and elevated native T1 values. The green arrow and relaxation curve refer to an area of normal septal myocardium and normal native T1 values. Images are sorted by inversion times.(Haaf et al., 2016)

Native (pre-contrast) T1 reflects a composite signal from both the intracellular (composed of mostly myocytes) and extracellular myocardial compartments (interstitium). Each tissue type exhibits a characteristic range of normal T1 relaxation times at a particular field strength, so, an alteration in these values may be indicative of disease or a change in physiology.(Karamitsos et al., 2020)

Thus, by encoding CMR images with actual T1 relaxation times, one could prescribe standardised cut-offs between “normal” and “affected” myocardium to eliminate observer-input in the delineation of diseased myocardium. (Messroghli et al., 2007)

Moreover, it is important to quantify native T1 values in all 16 myocardial segments and establish specific cut-off values for each of them. This, in fact, can contribute to an earlier and more precise diagnosis and to the quantification of the extent of cardiac involvement in various diseases. (Meloni, et al., 2021)

3. CLINICAL APPLICATIONS OF T1 MAPPING

The following graph shows the T1 map normal appearance and alterations in myocardial diseases [Figure 4], also resumed in Table II.

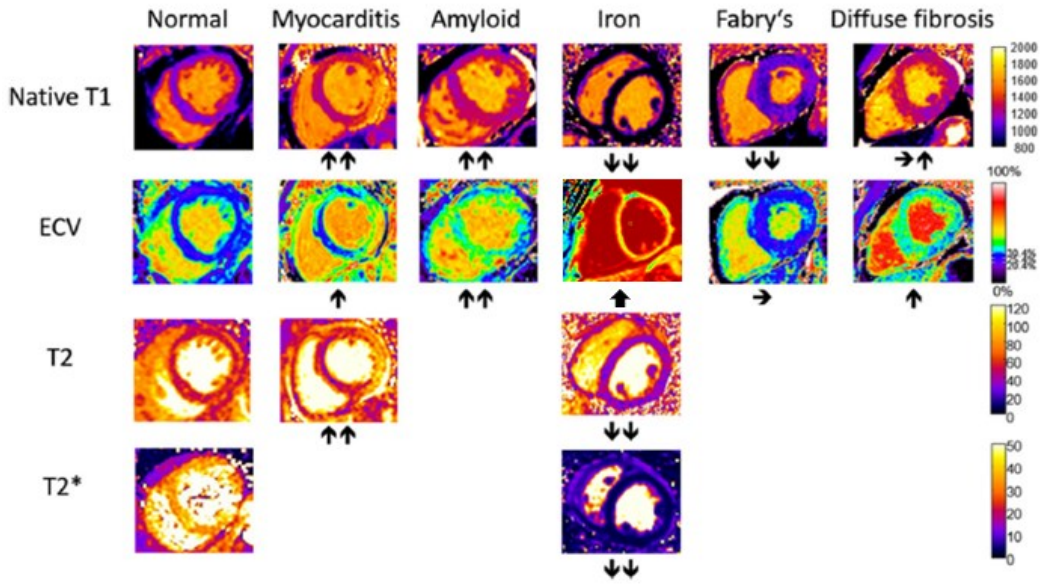

Figure 4: Typical appearance of T1, ECV, T2 and T2 maps in healthy subjects and in patients with myocardial* disease (adapted from Messroghli et al., 2017)

Table II: Typical alterations of T1, T2, T2 relaxation times and ECV in pathologic conditions* (Messroghli et al., 2017)

Measure	Decrease	Mild increase	Moderate or severe increase
Native T1	Anderson-Fabry, iron overload, fat, hemorrhage (athlete's heart)	diffuse fibrosis, scar, subacute inflammation	amyloid, acute inflammation, acute ischemia, necrosis
ECV	athlete's heart	diffuse fibrosis	amyloid, necrosis, scar
T2	iron, hemorrhage	subacute inflammation	acute inflammation, acute ischemia, necrosis
T2*	iron, hemorrhage, stress-induced		

3.1. ACUTE ISCHEMIC INJURY

Acute ischemic injury and infarction determine the development of myocardial oedema in the zone affected by the coronary occlusion. In those areas, native T1 and T2 relaxation times are prolonged, while post-contrast T1 relaxation time is shortened. ECV is high because of the presence of significant interstitial oedema. (Messroghli et al., 2017)

The highly prolonged T1 relaxation time relatively shortens during the chronic phase as oedematous and necrotic infarct tissue is replaced by fibrous scar.(Messroghli et al., 2007) Therefore, T1 mapping can be used as a reliable quantitative tool to discriminate between acute and chronic myocardial infarction.

Also, T2 weighted sequences permit discrimination between acute and chronic myocardial infarction as oedema resolves gradually and dissolves within 4–6 weeks. (Demirkiran et al., 2019)

The decrease of T1 post contrast is due to the obstruction of the microvascular circulation in the damaged tissue, with the abolition of perfusion, and consequently, contrast does not reach the zone. (Messroghli et al., 2007)

The elevation of native T1 and T2 could be useful to detect not only necrotic areas and their extent, but also helps to recognize the zones which may be saved with reperfusion and thrombolysis.

Native T1 mapping permits the evaluation of the severity of injury and prediction of myocardial recovery (Ma et al., 2021) and is able to distinguish between reversible infarction with oedematous myocardium and irreversible post-acute infarction with necrotic myocardium, as evaluated by late gadolinium enhancement, without the use of contrast.(Liu et al., 2017)

T1 mapping is superior to T2 weighted images for determining NSTEMI areas and as good as T2 weighted images for STEMI. (Dall'Armellina et al., 2012)

Post-contrast T1 and ECV changes have been identified in the remote myocardium early during acute infarction. Post contrast T1 tends to shorten in the non-

infarcted zones during the weeks after infarction. The expansion of the extracellular matrix starts early and then persists.(Chan et al., 2012)

This suggests that cardiac remodelling may start early at the time of infarction and is not only the result of long-term hemodynamic stress.(Messroghli et al., 2017)

Remote zone ECV is implicated in the pathophysiology of left ventricular remodelling. In STEMI survivors, an increase in remote zone ECV over time is associated with an increase in left ventricular end-diastolic volume, further implicating remote zone interstitial fibrosis in the pathophysiology of adverse cardiac remodelling. (Carberry et al., 2016)

3.2 ACUTE INFLAMMATION

Myocardial inflammation has different possible causes: ischemic injury, the immune response to viruses, autoimmune diseases, or toxic agents. CMR is important for non-invasive detection and exclusion of myocardial inflammation and has a role in determining prognosis.(Ferreira et al., 2018)

Due to the expansion of the interstitial space caused by acute myocardial inflammation, there is an increased amount of free water with oedema. Consequently, T1 and T2 relaxation times will be prolonged, as will ECV, due to the expansion of the interstitial space. (Messroghli et al., 2017)

Conventionally, T2 weighted sequences are used to detect myocardial oedema and inflammation, but the mapping techniques have superior diagnostic performance in this clinical setting.(Ferreira et al., 2013)

T1, T2 mapping and ECV are important for the diagnosis of acute myocarditis and should be used together, as they furnish complementary information. The update of the Lake Louise Criteria for myocardial inflammation indicates that CMR brings strong evidence for acute myocardial inflammation if at least one of the two following criterion is present: T2-based marker for myocardial oedema (T2 mapping or T2 weighted sequences), and T1-based marker for associated myocardial injury (LGE, T1 mapping and ECV).(Ferreira et al., 2018)

The mapping techniques are sensitive to less acute presentations of inflammation, for example, subclinical forms of myocarditis as parts of systemic inflammatory diseases such as rheumatologic disorders like rheumatoid arthritis, systemic lupus erythematosus, systemic sclerosis, spondyloarthropathies, vasculitis of small, medium, and large vessels, myositis, sarcoidosis, (S. Mavrogeni et al., 2022) pheochromocytoma, (Ferreira et al., 2016) and HIV-1 infection. (N. Ntusi et al., 2016)

3.2.1 SCLERODERMA

Scleroderma is a complex rheumatological disease that belongs to the group of diseases affecting the connective tissue. SSc is a rare systemic disease with many organs involved. The heart is one of the major organs involved, carrying the threat of sudden cardiac death, especially in diffuse cutaneous SSc. (Nie et al., 2019)

In the early stages there are reversible vasospastic and functional abnormalities without any clinical symptom(Kahan et al., 2009); then, as the disease progresses, the small coronary arteries present permanent structural abnormalities that cause microcirculation disturbances. Later in the development of SSc the myocardial fibrosis, that leads to diastolic and systolic disfunction, appears. (Kahan & Allanore, 2006)

Heart involvement in SSc is either primary, due to myocardial fibrosis, or secondary, due to pulmonary arterial hypertension (PAH) or systemic hypertension in patients with renal involvement. (Rodríguez-Reyna et al., 2014) Any structure of the heart may be affected in systemic sclerosis, leading to myocardial ischemia/fibrosis, pericarditis and myocarditis, conduction system defects, arrhythmias, valvular disease, and eventually heart failure. (S. I. Mavrogeni et al., 2017)

CMR is an important diagnostic tool in this pathology, as it allows the detection of oedema, infiltration, ischemia, and fibrosis of the myocardium, leading to early diagnosis of a cardiac involvement. (S. I. Mavrogeni et al., 2016)

SSc patients frequently have elevated native T1 values as determined by CMR, and these values are linked to inflammation, replacement fibrosis, and an enlarged LV. CMR T1 mapping seems to be a sensitive parameter to include in the routine clinical assessment of these patients to detect any cardiac worsening. (S. Mavrogeni et al., 2022)

In 50% of SSc patients, even those without cardiac symptoms or pathological findings at echocardiography or conventional CMR, native myocardial T1 mapping enables the discovery of left ventricular increased T1 values, most frequently linked to diffuse myocardial fibrosis. (Poindron et al., 2020)

Both native T1 mapping and ECV represent novel non-invasive markers of diffuse myocardial fibrosis/oedema and could be used in the risk stratification of patients with SSc. CMR mapping may provide a novel biomarker for disease monitoring and tailoring the therapies. (Bordonaro et al., 2021)

Native T1 mapping and ECV quantification permit the detection of areas of T1 abnormality and expanded ECV due to a combination of low-grade inflammation and diffuse myocardial fibrosis. T1-mapping and ECV quantification allow for further stratification of myocardial involvement in patients with diffuse SSc compared to patients with the limited cutaneous form, with the former showing significantly larger areas of myocardial T1 abnormality and ECV expansion. T1 and ECV measures could also be associated with slight myocardial systolic and diastolic dysfunction. (N. A. Ntusi et al., 2014)

CMR may contribute to early assessment and treatment guide in SSc, due to its capability to perform tissue characterization, compared to other imaging techniques. (S. I. Mavrogeni et al., 2017)

In particular, T1 and ECV quantification could be used for early detection of subclinical myocardial involvement, potentially serving as an early diagnostic tool before evident LV dysfunction or irreversible myocardial damage occurs.(N. A. Ntusi et al., 2014)

3.3 ANDERSON-FABRY DISEASE

Anderson-Fabry disease (AFD) is a rare X-linked lysosomal storage disorder caused by α-galactosidase enzyme deficiency. The consequences are multisystemic, with a progressive intracellular accumulation of glycosphingolipids in the endothelium and smooth muscle.

Classic AFD causes diverse clinical features: skin disorders, corneal alterations, cerebrovascular complications, kidney failure, and cardiovascular disease, particularly left ventricular pseudo-hypertrophy.

Cardiac disease in the Anderson-Fabry is correlated to an accumulation of glycosphingolipids in all cellular components of the heart, including cardiomyocytes, conduction system cells, valvular fibroblasts, endothelial cells, and vascular smooth muscle cells.

Cardiovascular involvement is the major cause of morbidity and mortality, and it consists of left ventricular pseudo-hypertrophy, which eventually leads to fibrosis and heart failure. Also, valvular dysfunction, arrhythmias, and coronary artery disease could be significant complications. (Ponsiglione et al., 2022)

CMR is the most important non-invasive imaging modality for cardiac involvement in this disease. Native T1 values are low due to cardiac glycosphingolipid overload, and, in early stages, this could precede the development of left ventricular pseudo-hypertrophy and the consequential disfunction.

T1 mapping values are useful to detect early cardiac involvement, being low in around half of the patients even in the absence of hypertrophy, and as diagnostic tool in predicting disease progression without using gadolinium-based contrast medium, which could be problematic in patients with severe kidney involvement. (Messroghli et al., 2017)

A decreased T1 value represents a characteristic feature that can help distinguish AFD from other cardiomyopathies with a hypertrophic phenotype.(Kim et al., 2017)

Recognition and quantification of myocardial replacement fibrosis by late gadolinium enhancement is an important prognostic feature. There is a characteristic LGE pattern in the basal inferolateral wall, which often appears thin. This area can present increased T2 values correlated to elevated levels of troponin in the blood, thus suggesting the presence of chronic active inflammation. Thus, in the infero-lateral wall it is possible to find a pseudo-normalization for the T1 values due to a relatively high T1 values for oedema/diffuse fibrosis. ECV seems to be not variated in Anderson-Fabry disease. (Thompson et al., 2013)

3.4 IRON OVERLOAD

Iron overload might be caused by a hereditary disease such as hemochromatosis, characterised by increased intestinal iron absorption, or may be secondary to several pathologies in which repeated blood transfusions are required causing iron accumulation, such as haemoglobinopathies like thalassemia major (TM), or haematological diseases such as myelodysplasia. Because there is no physiological mechanism to discard it, the organism tends to retain iron and accumulate it in the tissues as a result of repeated blood transfusions. Cardiac iron overload leads to severe heart failure and arrhythmias but may be treated effectively if diagnosed early. (Pepe et al., 2022)

The presence of iron deposits causes a lowering of the values of T1, T2 and T2*, as it creates microscopic magnetic field inhomogeneities. (Meloni, et al., 2021)

The best technique for cardiac iron quantification is T2*, as it is fast, reproducible, (Ramazzotti et al., 2009) and it is the first parametric mapping technique that has become a clinical tool and reference method, (Meloni et al., 2020) and it may be used to monitor disease progression and therapy (Pepe et al., 2018). Moreover, the T2* segmental approach allows the non-invasive measurement of myocardial iron and represents an early and sensitive way to quantify it (Pepe et al., 2020).

Also, the use of native segmental T1 combined with T2* can improve the sensitivity for detecting myocardial iron overload. Native T1 mapping seems to be a more sensitive marker of myocardial iron overload compared to T2* mapping,

although it is less specific given that diffuse fibrosis can increased T1 values. Moreover, it seems to be also a useful marker of cardiac complications in patients with β-thalassemia major. (Meloni, et al., 2021) Myocardial iron overload by cardiovascular magnetic resonance native segmental T1 mapping: a sensitive approach that correlates with cardiac complications)

Also, for T1 mapping, the segmental approach permits detection of an early and heterogeneous iron distribution that otherwise would not have been recognised with a single measurement in the mid ventricular septum. (Meloni, et al., 2021)

ECV is increased in patients with thalassemia major and is associated with iron overload and heart failure. (Meloni et al., 2022)

Iron-induced cardiomyopathy is reversible if intensive chelation therapy is instituted in time, so mapping technique are mandatory for tailoring the chelation therapy and for opening the prognosis. (Pepe et al., 2018)

3.5 MYOCARDIAL FIBROSIS

Myocardial fibrosis is a common feature of many cardiac diseases. It could be focal or diffuse and is associated with a poor prognosis for major adverse cardiovascular events. It could vary from mild to severe, where the excess of collagen occupies the myocardial interstitium.

There are two main types of myocardial fibrosis: reactive interstitial fibrosis and replacement fibrosis. (Karamitsos et al., 2020)

Reactive interstitial fibrosis is characterised by a diffuse microscopic distribution, sometimes perivascular. It is reversible if the causes are treated promptly, otherwise it degenerates into irreversible replacement fibrosis.

Replacement fibrosis is characterised by myocyte apoptotic death, which stimulates fibroblast activation and the deposition of collagen.

Myocardial native T1 increases in the areas of fibrosis as there is an increment of free water in the tissue. ECV also increases and is well suited to measure interstitial

expansion occurring with fibrosis with extracellular gadolinium-based contrast agents. (Messroghli et al., 2017)

ECV is a surrogate marker of fibrosis when other diseases that increase the extracellular space, such as myocardial oedema or inflammation, infiltration, and ischemia, have been excluded. (Karamitsos et al., 2020)

The two possible patterns of fibrosis distribution are: focal or diffuse. Focal fibrosis is usually represented by the areas of focal replacement fibrosis in chronic myocardial infarction and shows high native T1 values and ECV. Also, non-ischemic heart disease areas of focal fibrosis seen on LGE have high T1 and ECV values. (Karamitsos et al., 2020) Diffuse fibrosis identification and quantification is allowed by T1 mapping and ECV techniques and shows good correlation to collagen volume fraction. (Karamitsos et al., 2020). Late gadolinium enhancement imaging, instead, has limitations for detecting diffuse myocardial fibrosis because it requires regions of presumed normal myocardium to have a comparison between affected and unaffected tissue, which may not be available in diffuse pathology.

Moreover, ECV has been shown to be reproducible, predict outcomes and provide “added prognostic value”. Thus, ECV quantification of interstitial expansion remains a powerful tool to investigate myocardial remodelling. (Messroghli et al., 2017)

3.6 AMYLOIDOSIS

The term “amyloid” is used to describe anomalous extracellular, insoluble, protein fibrils that resist proteolysis and infiltrate many organs, such as the heart, kidney, and liver.

Cardiac amyloidosis is characterized by extracellular amyloid infiltration, which causes impairment of myocardial contractile function and electrical conduction. (Karamitsos et al., 2020)

There are two main types of amyloidosis that affect the myocardium: immunoglobulin light-chain derived amyloidosis (AL) and transthyretin (ATTR) amyloid. They have different behaviour and prognosis, but in both, the cardiac involvement is the one which guides the clinical and therapeutical choices. (Messroghli et al., 2017)

ATTR amyloidosis can be acquired, linked to wild-type transthyretin (previously known as senile systemic amyloidosis), or hereditary, associated with variants in the transthyretin gene. (Gillmore et al., 2016)

Systemic amyloid light-chain (AL) amyloidosis is a multiorgan, infiltrative disorder caused by a plasma cell dyscrasia that leads to overproduction of immunoglobulin light chains and is characterized by tissue and organ amyloid deposition with interstitial expansion. (Banypersad et al., 2015)

There are different clinical features: heart failure symptoms prevail, but also syncope, arrhythmias, or unexplained left ventricular wall thickening on echocardiography may be present. (Gillmore et al., 2016)

Cardiac immunoglobulin AL amyloidosis and transthyretin amyloidosis can be detected by a circumferential pattern of LGE in combination with a dark blood pool (for the AL form), which usually affects the subendocardium at the beginning and then expands transmurally in the left and right ventricles as the disease progresses. (Karamitsos et al., 2020)

If there is also a severe renal involvement, it is suggested for restricting the use of contrast, so native T1 mapping may help with this, aiding the diagnostic process without using gadolinium-based contrast medium. (Messroghli et al., 2017)

T1 mapping has high diagnostic accuracy for detecting cardiac amyloidosis and greater sensitivity for detecting early disease compared to LGE-CMR. (Karamitsos et al., 2020)

In early disease, native T1 and ECV are elevated before LGE, even though these changes are initially non-specific and thus only useful when the pre-test probability is high. When subendocardial LGE appears, the ECV rise in isolated

areas begins to be diagnostic, as diffuse fibrosis rarely increases the ECV above 40%. In transmural LGE, ECV could be over 55%. (Messroghli et al., 2017)

In established AL vs. ATTR, the T1 and ECV are slightly different, with a higher ECV in ATTR and a higher native T1 in AL. (Fontana et al., 2015)

ECV adds incremental value over and above existing clinical markers when risk stratifying patients with AL.(Banypersad et al., 2015)

The degree of ECV expansion in cardiac amyloidosis is beyond that of any other myocardial disease, making it almost pathognomonic, especially when combined with structural, functional, and clinical features. (Karamitsos et al., 2020)

As a direct assessment of the cardiac interstitium, myocardial extracellular volume is likely a surrogate marker of amyloid burden. It can also determine the amount of amyloid in other organs. (Banypersad et al., 2015)

Myocardial native T1-mapping and ECV predict mortality in patients with systemic amyloidosis. (Karamitsos et al., 2020) ECV has prognostic significance, can be used to monitor amyloid therapy, and may be able to monitor amyloid regression. (Messroghli et al., 2017)

3.7 ATHLETE'S HEART

Athletes who frequently undertake high intensity exercise can develop changes in cardiac structure and function because of physiological adaptation to exercise. Two main features are characteristic: a slow heart rate and an enlargement of the heart.(Galderisi et al., 2015)

"Athlete's Heart" may overlap with some features of pathological conditions such as dilated cardiomyopathy, hypertrophic cardiomyopathy, or isolated left ventricular non-compaction.(Brosnan & Rakhit, 2018)

T1 and T2 mapping are potentially useful tools to differentiate between an Athlete's Heart and dilated non-ischemic cardiomyopathy and could be used if standard techniques fail to differentiate them. In DCM (Dilated Cardiomyopathy),

native T1 and T2 are longer, post-contrast T1 is shorter, and ECV values are higher. (Mordi et al., 2016)

A differential diagnosis with hypertrophic cardiomyopathy must also be made as athletes have physiological left ventricular hypertrophy due to an increase in the size of the myocytes while maintaining normal or decreased values of ECV. So, ECV permits us to distinguish between athletic and pathological hypertrophy, as the first is not related to an increase in extracellular volume. (Swoboda et al., 2016)

4. NORMAL VALUES IN HEALTHY SUBJECTS

In healthy subjects, myocardial tissue has a uniform composition and possesses homogeneous magnetic properties. Consequently, the native T1, T2 and T2* values of a normal myocardium are highly reproducible and, when acquired under the same conditions, also have very narrow ranges. (Messroghli et al., 2017)

However, these conditions are varied and heterogeneous: firstly, the use of different sequences and different methods of generating the maps lead to important variations in the values obtainable from the mapping. Added to this is also the variability determined by the scanner used to acquire the images and by the analysis program used to evaluate the maps. Usually, there is a prolongation of average global T1 relaxation times, either native T1 or post-contrast T1, and a reduction of T2 values at 3 T compared to 1.5 T (Granitz et al., 2019). ECV is not affected by field strength if we use the same contrast agent at an equimolar dose. (Kawel et al., 2012)

Other concomitant factors, secondary to those mentioned above, are possible alterations in the body temperature of the subject in question. For example, the relaxation time T1 increases by about 1% for every 1°C increase in body temperature (Peller 2003) while as body temperature increases the relaxation time T2 decreases, which makes the investigation less suitable in patients with fever or hypothermia. Furthermore, local variations in the magnetic field lead to reduced reproducibility between different centres.

As a result of the previous considerations, obtaining normal values as a reference for each centre represents a useful investment of resources and time aimed at improving the diagnostic accuracy and capacity of the centre itself. The current consensus documents recommend a minimum number of 20 healthy volunteers to be able to use the mapping techniques, but at least 50 healthy volunteers to be able to exploit these techniques in all their power of tissue characterization. (Messroghli et al., 2017)

Therefore, it is important for a centre to obtain normal values as a reference for their studies; in fact, doing so goes a long way toward improving diagnostic accuracy.

To the best of our knowledge, this is the first study that evaluate 16 segmental and global T1 normal values with a 1.5 T Siemens scanner, using MOLLI sequences analysed with cvi42 software in a large study population stratified for sex and age.

AIM OF THE STUDY

The purpose of the study was to assess the global T1 value and the variability of T1 relaxation time among the 16 cardiac segments, to evaluate their association with sex, age, wall thickness, and cardiac phase (systole and diastole) in 50 healthy subjects stratified by sex and age. Then, we applied the reference values obtained in our own Institute, compared to literature values, in same illustrative cases for testing the value of sex and age specific normal cut off values for classifying health versus disease.

MATERIALS AND METHODS

1. POPULATION OF THE STUDY

Fifty healthy subjects (M: F=1:1) were prospectively recruited between November 2021 and September 2022.

The inclusion criteria were age between 20 and 69 years old; absence of cardiovascular risk factors such as smoking, dyslipidaemia, hypertension, diabetes, obesity, family history for cardiovascular diseases; normal EKG performed in the previous one month; no contraindication to Magnetic Resonance; no history of cardiovascular symptoms or systemic pathology or SARS-CoV-2 infection in the last three months. Also, the SARS-CoV-2 vaccinal cycle had to be completed at least in the previous three months.

These criteria were verified by the anamnestic collection, ruled out with a lifestyle questionnaire, also assessing body mass index and body surface area, for anthropometric analysis. If a recent EKG was not available, it was performed right before the CMR.

Patients were included with a stratified approach by sex and age: 5 men and 5 women were selected for each age decade from 20 to 69 years old (i.e., 20-29, 30-39, 40-49, 50-59, and 60-69). If one subject had to be excluded due to an incompatibility with all the above-mentioned criteria, or due to a pathological finding at the MR, they were replaced with another subject of the same gender and age group.

The patients underwent CMR in the months of April, May, and September 2022.

All volunteers had a normal 12-lead EKG and all the CMR scans were reported to be normal by a 22 years-experienced CMR radiologist and cardiologist (A.P.).

The study complied with the Declaration of Helsinki and was approved by the institutional Ethical Committee. All the patients enrolled received information regarding the protocol and signed informed consent.

2. CARDIAC MAGNETIC RESONANCE PROTOCOL

All Cardiac Magnetic Resonance were performed using a 1.5T Siemens MAGNETOM Avanto Fit scanner (software: syngo MR E11) with a 32-channel cardiac phased array receiver.

Initially, scout images were acquired to localize the long and short axis of the left ventricle, then cine SSFP 2-, 4-, and 3-chamber images were acquired to localize the mapping sequences (8 mm thick and 30 phases per beat).

Three parallel short-axis slices (basal, medial, and apical) of the left ventricle were acquired with breath-holding MOLLI sequences at the end of exhalation and with cardiac gating in telediastole and in telesystole phase.

T1 mapping was performed using an imaging technique based on inversion recovery with a 5(3)3 prototype (5 acquisition heartbeats followed by 3 recovery heartbeats and a further 3 acquisition heartbeats) on 3 short-axis slices (basal, mid-ventricular, and distal). The acquisitions are synchronised with the same cardiac phase and thus enable pixel based T1 value estimation in the myocardium.

The T1 sequence parameters were as follows: inversion time (TI) = 190 ms, FoV read ≥ 350 mm, basal resolution = 256. The acquisition parameters were as follows: cross-section thickness = 8mm, flip angle (α) = 35°; bandwidth = 1085 Hz/Px, matrix = 125x256 pixel.

A subpopulation comprising one subject per gender per age group repeated the cardiac MRI protocol within one hour from the first acquisition. The T1 image sets were blindly analysed by the candidate to assess inter-study reproducibility.

3. IMAGES ANALYSIS

Native T1 and SSFP images were transferred to cvi42 software (Circle Cardiovascular Imaging Inc., Version 5.14.2, Calgary, Alberta, Canada) for post-processing analysis; the short-axis images were also analysed to obtain the parietal segmental thickness of myocardial segments 7-12.

The image analysis has been performed personally by the candidate with the partnership of a radiology Ph.D. (A.L.) and under the supervision of a cardio-radiologist with 22 years of experience (A.P.).

The T1 maps [Figure 5] were generated from the native images during the acquisition phase. By acquiring a series of images at different T1 times, the T1 relaxation curve was calculated and a pixelwise based T1 map with motion correction was generated.

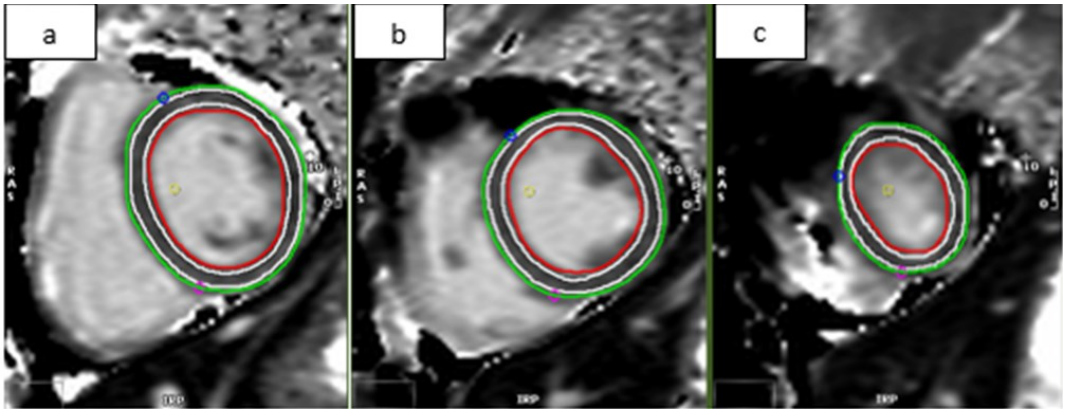

Figure 5: T1 maps of the basal (a), mid-ventricular (b), and distal (c) sections of the left ventricle evaluated by the cvi42 software. The epicardial limit is traced in green, while the endocardial limit is indicated in red. The white line represents the correction off-set of 20%.

For each short axis slice, endocardial and epicardial borders are automatically traced on the corresponding T1 map using a specific artificial intelligence function of the cvi42 software, and then verified by human's eye carefully avoiding blood pool and epicardial fat inclusion. To guarantee greater homogeneity and avoid partial volume effects, an off-set erosion of 20% was applied to both the endocardial and epicardial borders using a function provided by the software. The resultant borders were verified by a cardio-radiologist with 22 years of CMR experience (A.P.).

Finally, the T1 segmental values map, according to AHA classification, is obtained. [Figure 6].

For each slice, the T1 value in each segment represents the average of T1 values for all the pixels within the segment. If there was an evident artefact due to

cardiorespiratory motion, susceptibility, or partial volume effects, that could alter the segmental value, the corresponding segment was not considered for statistical analysis. T1 global values result from the average of all segmental T1 values.

The segments were considered also according to their sections for further analysis (i.e., basal: segments 1-6; medial: segments 7-12; distal: segments 13-16).

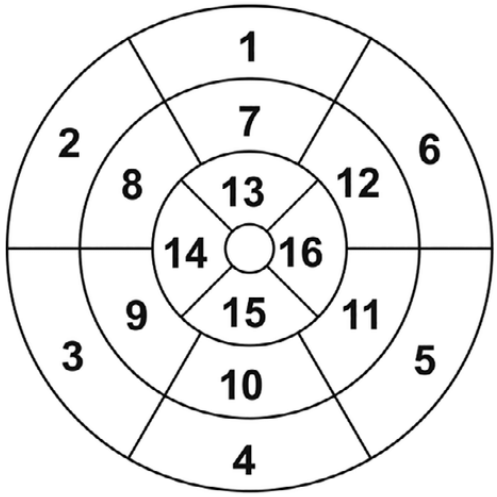

1: basal anterior
2: basal antero-septal
3: basal infero-septal
4: basal inferior
5: basal infero-lateral
6: basal antero-lateral
7: mid anterior
8: mid antero-septal
9: mid infero-septal
10: mid inferior
11: mid inferolateral
12: mid anterolateral
13: distal anterior
14: distal septal
15: distal inferior
16: distal lateral

Figure 6: Bullseye representation of the 16 myocardial segments according to AHA classifications.

4. STATISTICAL ANALYSIS

R and associated statistical supplements were used to analyse all data.

Continuous variables were defined as mean ± standard deviation (SD), while categorical variables were defined as frequencies and percentages.

The normality of the parameter distribution was confirmed using the Shapiro-Wilk test for a sample size of $n \leq 50$. Comparison between two groups was performed with a t-test for independent samples or the Mann-Whitney test for continuous variables.

One-way ANOVA or Kruskal-Wallis tests were used to assess differences among T1 values in myocardial sections; post-hoc Bonferroni test was applied in all comparisons between couples.

Where appropriate, Pearson's or Spearman's test were used to analyse the correlation between T1 values and study population characteristics, such as age, sex, and wall thickness.

The lower and upper limits of normality for T1 values were calculated on the original data and shown as mean (μ) ± 2 SD.

A two-tailed $p<0.05$ was considered statistically significant.

4.1. REPRODUCIBILITY ANALYSIS

To assess repeatability, a subpopulation of 10 subjects (i.e., comprising one subject for each age group and gender) underwent another CMR acquisition within one hour from the first one. The two sets of T1 images have been personally and blindly analysed to evaluate the inter-study reproducibility.

The first set of 10 exams in those specific subjects were personally and blindly analysed a second time after one week to evaluate the intra-observer reproducibility. The same set of images has also been observed by another operator (i.e., radiology Ph.D.) to evaluate the inter-observer reproducibility.

A paired t test or a Wilcoxon signed rank test were used to find statistically significant differences in the context of inter-study, inter-observer, and intra-observer reproducibility ($p< 0.05$).

Intra-class correlation (ICC) was measured to evaluate the correlation between the different datasets to ascertain inter-study, intra-observer, and inter-observer reproducibility. An ICC between 0.75 and 1 suggests excellent correlation; an ICC between 0.60 and 0.74 suggests good correlation; a value less than 0.40 suggests poor correlation.(Bunting et al., 2019)

Concordance between inter-study, inter-observer, and intra-observer measurements was assessed using Bland-Altman analysis to check for systematic bias and to calculate 95% limits of agreement.

4.2. VARIABILITY ANALYSIS IN RELATION TO THE CARDIAC PHASE

In all the subjects under examination, sequences in the end-diastolic and end-systolic phase were acquired, in order to determine the presence of statistically significant differences between the two sets of images.

Similarly, to the reproducibility analysis, t-tests for paired data or Wilcoxon-signed rank tests, based on the normality of the data, were performed. The agreement between the measurements was assessed using the Bland-Altman analysis, and the intra-class correlation (ICC) was calculated.

RESULTS

1. STUDY POPULATION

A population of 53 healthy subjects underwent CMR scan. Three subjects were excluded for abnormalities found at CMR examination: one subject (male, 67 years old) showed findings compatible with hypertrophic cardiomyopathy; another subject (female, 54 years old) showed signal alterations compatible with adipose infiltration/metaplasia of the distal interventricular septum; another subject (female, 58 years old) showed MR findings compatible with myocarditis (significantly high native T1 and T2 mapping values and positive TIRM T2 with a non-ischemic pattern). They were all replaced by another healthy subject of the same gender and decade.

All the 50 healthy volunteers included were Caucasian. Table III shows the population average ages divided by sex and the average segments thickness. The average wall thickness measured in tele-diastole was between 5.2 mm (mid-ventricular infero-lateral segment) and 6.6 mm (mid-ventricular infero-septal segment). The left ventricular wall thickness was shown to be significantly higher in male subjects in all myocardial segments ($p < 0.001$).

Table III: Differences between males and females mean age and mid-ventricular wall thickness

	Males (N=25)	**Females (N=25)**	**p value**
Age	43.7 ± 14.2	42.6 ± 14.2	0.683
Mid-ventricular wall thickness (mm)			
7: mid-ventricular anterior	6.8 ± 1.1	5.1 ± 1.3	< 0.001
8: mid-ventricular antero-septal	7.1 ± 1.2	5.3 ± 1.0	< 0.001
9: mid-ventricular infero-septal	7.5 ± 1.2	5.7 ± 0.8	< 0.001
10: mid-ventricular inferior	6.3 ± 1.3	4.6 ± 1.1	< 0.001
11: mid-ventricular infero-lateral	6.0 ± 1.3	4.4 ± 1.0	< 0.001
12: mid-ventricular antero-lateral	5.8 ± 1.0	4.7 ± 0.8	< 0.001

2. REPRODUCIBILITY ANALYSIS

A subset of 5 males and 5 females (one each for age decade) was analysed to assess the reliability of acquired data. Fourteen segments belonging to 5 patients were excluded from the analysis, due to artifacts.

Globally, no statistically significant differences were found between means ($p>0.05$).

The global ICC for the inter-study, intra-observer, and inter-observer correlation was found to be 0.80, 0.90, and 0.80 respectively.

Bland-Altman plots for global T1 values are shown in Figure 7.

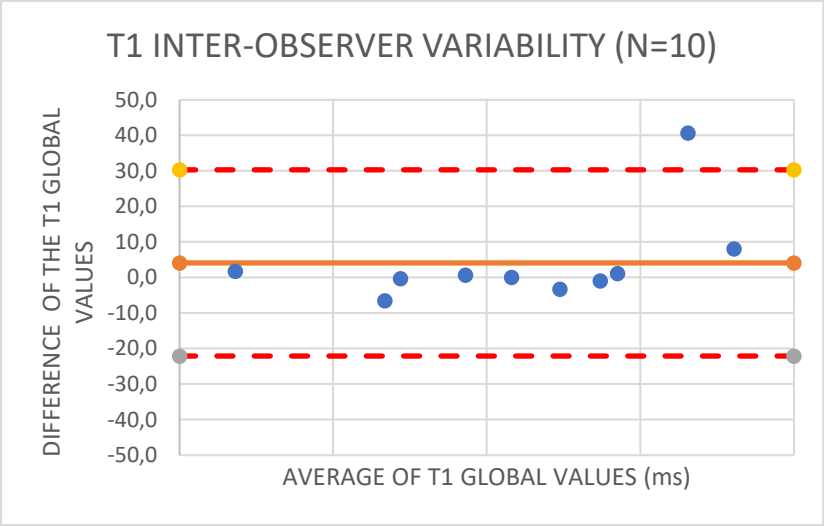

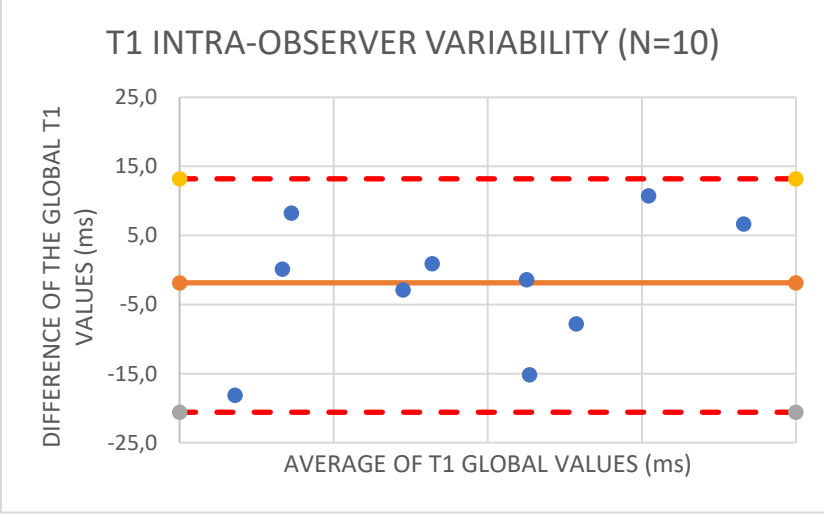

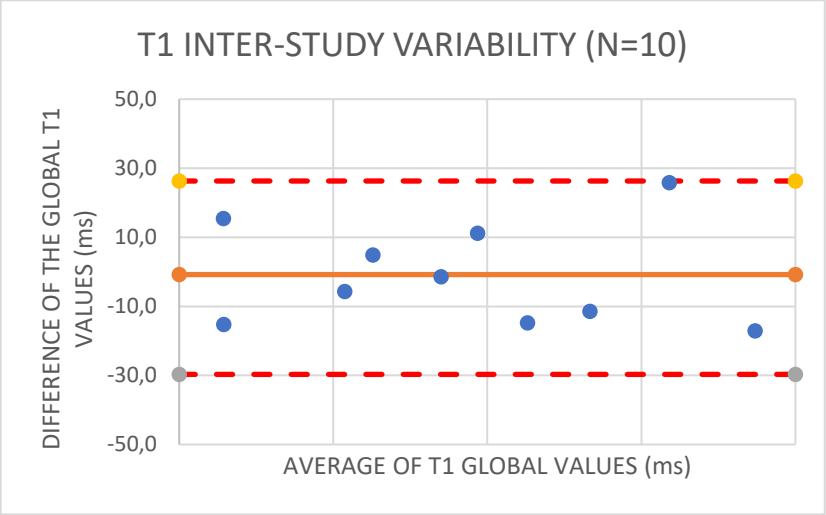

Figure 7: Bland-Altmann limits (dotted lines) for the inter-observer, intra-observer, and inter-study reproducibility of T1 global values.

3. SEGMENTAL VARIABILITY OF T1 VALUES.

The overall average T1 value of all healthy subjects turned out to be 993.2 ± 24.0 (range 945.2-1041.2 ms).

The lowest average T1 value was measured at the level of the mid-ventricular anterior segment (978.4 ms, segment 7 in Figure 8), while the highest average value was measured in the basal inferior segment (1010.9 ms, segment 4 in Figure 8).

No significant difference emerged between sections (basal vs mid-ventricular p=0.4; mid-ventricular vs apical p=0.8; basal vs apical p=0.8) considering all subjects [Figure 9]. In males only, the comparison between basal and mid-ventricular sections showed a significant difference, with lower values in the latter (p=0.01); no statistically significant differences were found between the mid-ventricular and the distal sections (p=0.8) or between the basal and the distal sections (p=0.1) [Figure 10]. In females only, no significant difference emerged between the sections (i.e., basal vs mid-ventricular p=0.1; mid-ventricular vs apical p=0.7; basal vs apical p=0.4) [Figure 11].

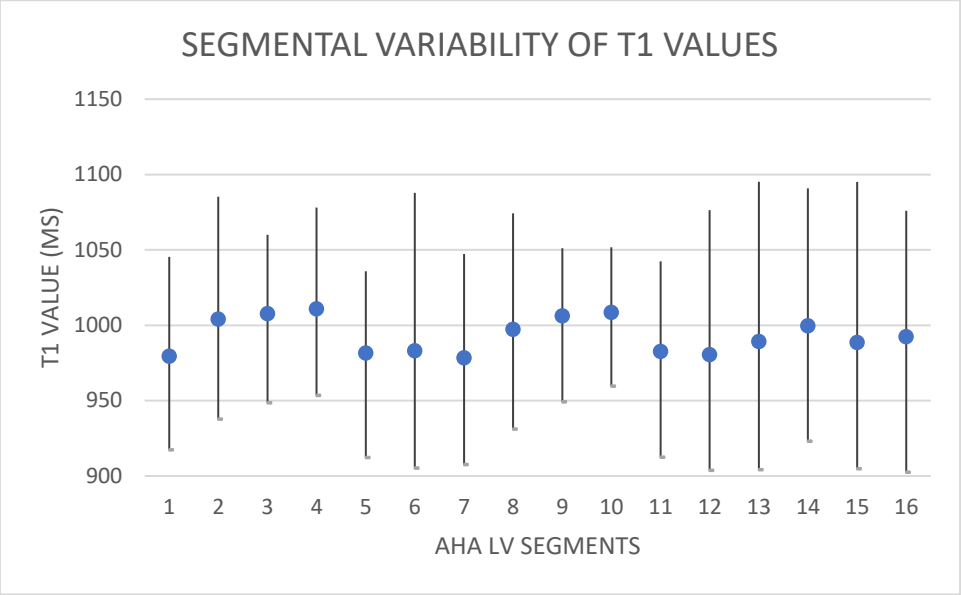

Figure 8: T1 relaxation times (ms) in the 16 AHA segments (mean ± SD).

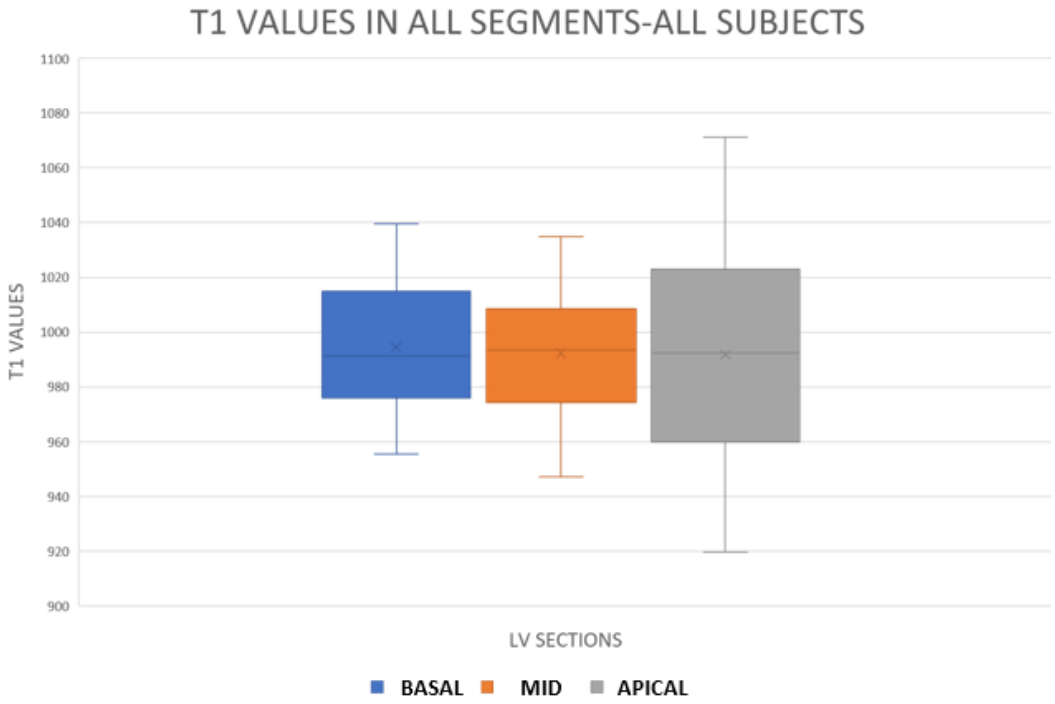

Figure 9: Average T1 values for the basal, mid-ventricular, and distal segments for all subjects.

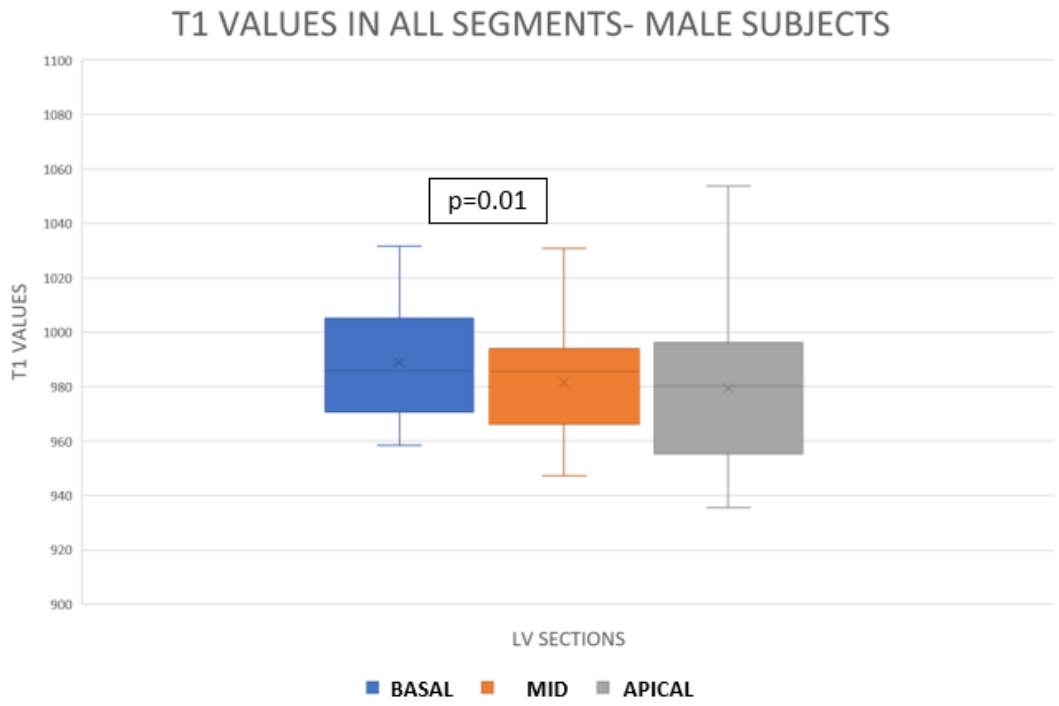

Figure 10: Average T1 values for the basal, mid-ventricular, and distal segments for male subjects.

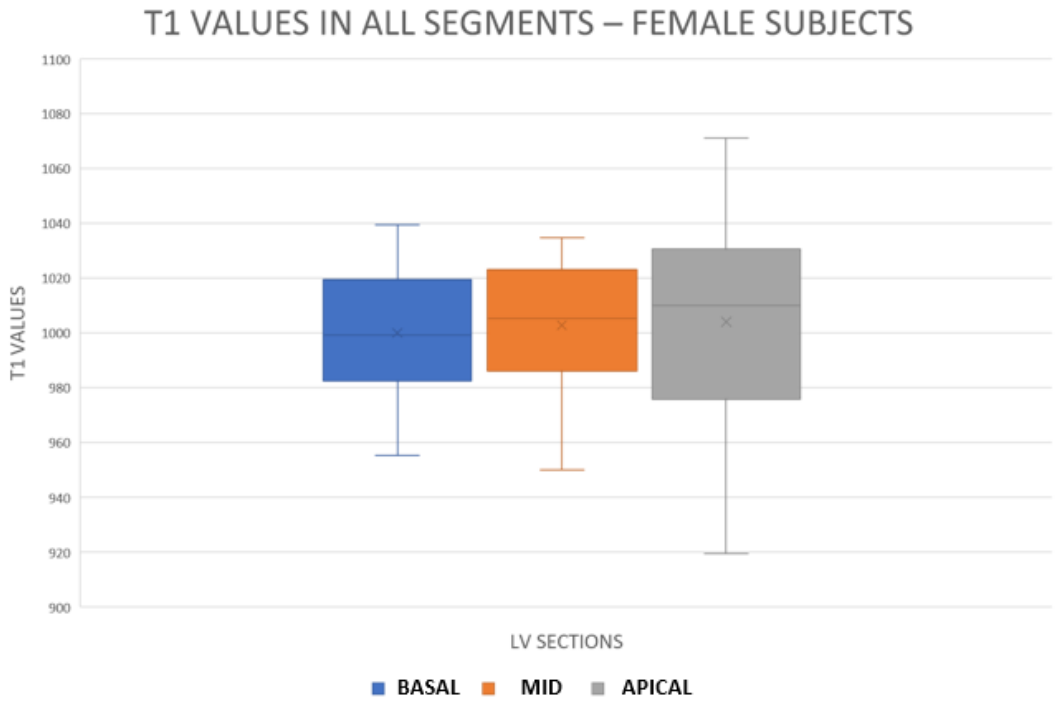

Figure 11: Average T1 values for the basal, mid-ventricular, and distal segments for female subjects.

When comparing the segmental values between males and females, no difference was found in the basal section (p=0.1), while middle and distal sections showed significantly lower values in males, (p=0.001 and p=0.009, respectively. [Figure 12]

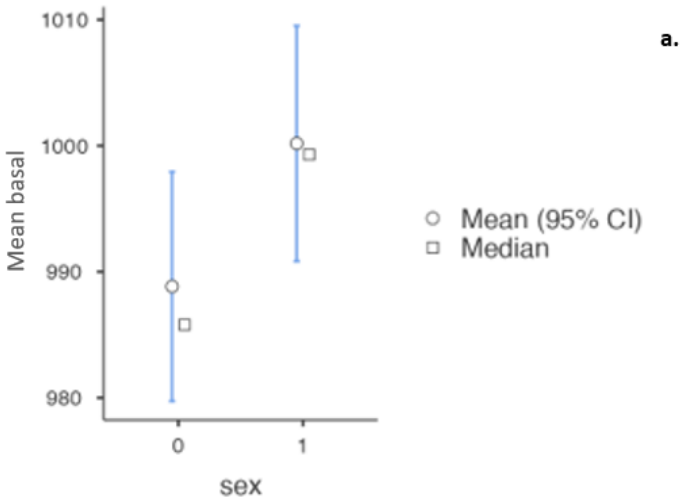

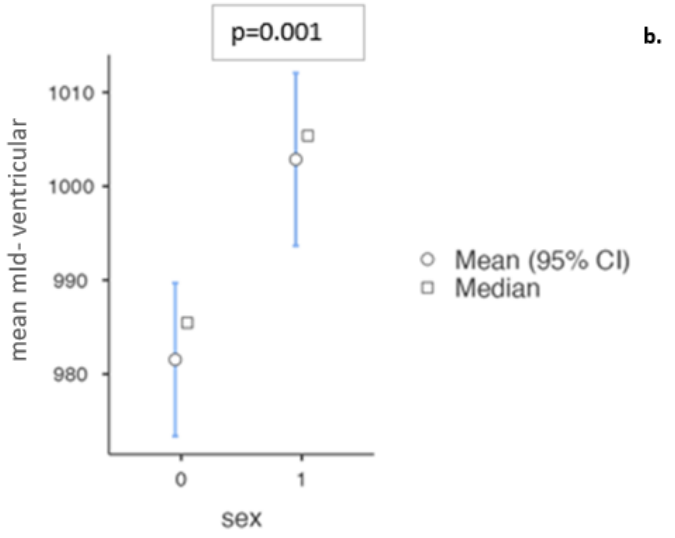

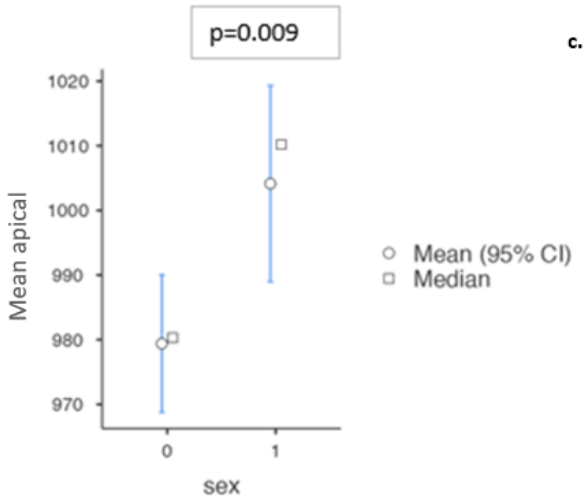

Figure 12: 0=MALES, 1=FEMALES. Mean T1 values for basal (a), mid-ventricular (b), and distal (c) segments for males and females. No statistically significant difference was found in the basal segment.

An example of a T1 map is visible in figure 13.

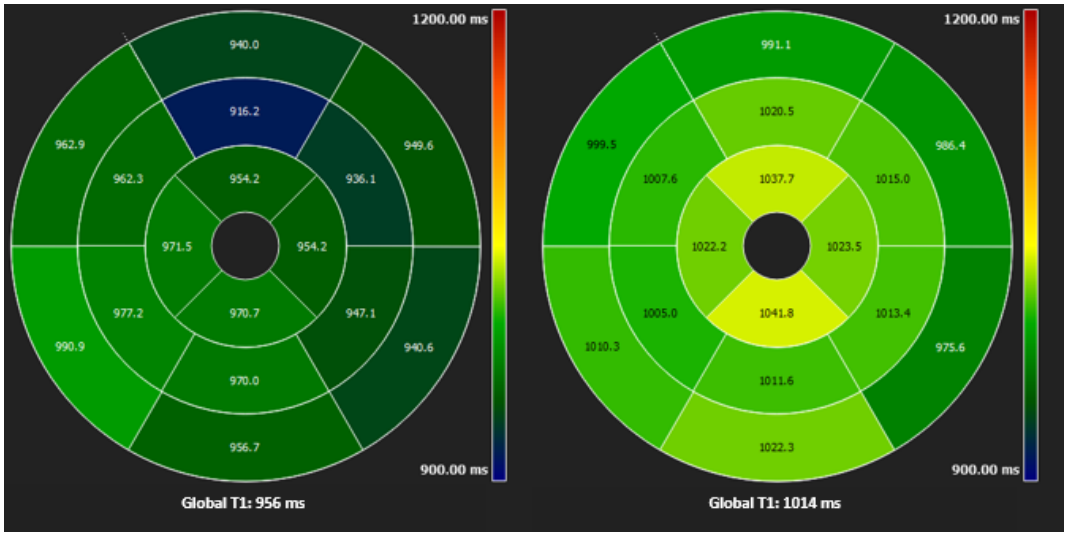

Figure 13: example of a "Bull's-eye" map obtained from T1 mapping sequences. A male and female subject of the same decade (i.e., 20-29 years old) T1 mapping values, on the right and left side, respectively

4. T1 VALUES AND POPULATION CHARACTERISTICS

Table IV illustrates the association between native T1 measured values and the characteristics of the population enrolled (i.e., age, gender, and wall thickness).

Statistical correlation analysis of the overall global T1 values and age of the subjects revealed a weak statistical correlation (R= 0.279; p= 0.050). Considering the segmental values instead, there was a statistically significant correlation in two segments.

The overall measured T1 values were lower in male than in female subjects (983.8 ± 20.5 vs 1002.5 ± 23.9; p= 0.004) [Figure 14].

A statistically significant difference between the two genders was found in the following segments: basal inferior, mid-ventricular anteroseptal, infero-septal, inferior, infero-lateral, and antero-lateral, distal septal, inferior, and lateral.

The study of the correlation of segmental T1 values with wall thickness was performed on the mid-ventricular, and no correlation was found.

Table IV: influence of physiological parameters on T1 values.

segments	correlation with age [R ; p value]		comparison of the T1 values in male and female subjects (p value)		correlation with wall thickness [R ; p value]
1: basal anterior	R='-0.248	p= 0.082	975.5 ± 29.3 vs 983.4 ± 29.2	p= 0.323	N/D
2: basal antero-septal	R= 0.278	p= 0.051	998.4 ± 36.5 vs 1010.1 ± 30.9	p= 0.115	N/D
3: basal infero-septal	R= 0.180	p= 0.210	1003.2 ± 28.9 vs 1012.2 ± 23.7	p= 0.200	N/D
4: basal inferior	R= 0.049	p= 0.737	1001.9 ± 31.8 vs 1019.9 ± 23.7	**p= 0.019**	N/D
5: basal infero-lateral	R= 0.125	p= 0.386	978.6 ± 33.6 vs 984.7 ± 35.6	p= 0.509	N/D
6: basal antero-lateral	R= 0.095	p= 0.513	975.5 ± 22.2 vs 990.9 ± 37.8	p= 0.095	N/D
7: mid-ventricular anterior	R= 0.383	p= 0.060	970.3 ± 32.1 vs 986.6 ± 33.9	p= 0.092	R= 0.049; p= 0.733
8: mid-ventricular antero-septal	R= 0.404	**p= 0.004**	986.3 ± 27.7 vs 1008.6 ± 32.7	**p= 0.007**	R='-0.147; p= 0.307
9: mid-ventricular infero-septal	R= 0.175	p= 0.225	995.3 ± 20.8 vs 1017.3 ± 23.4	**p= 0.001**	R='-0.172; p= 0.232
10: mid-ventricular inferior	R= 0.003	p= 0.986	996.6 ± 26.0 vs 1020.3 ± 19.6	**p= 0.001**	R= 0.025; p= 0.862
11: mid-ventricular infero-lateral	R= 0.173	p= 0.235	974.5 ± 25.0 vs 990.6 ± 31.5	**p= 0.036**	R= 0.028; p= 0.849
12: mid-ventricular antero-lateral	R= 0.055	p= 0.702	967.6 ± 27.9 vs 993.8 ± 38.3	**p= 0.003**	R='-0.187; p=0.194
13: apical anterior	R= 0.170	p= 0.242	983.5 ± 46.8 vs 995.4 ± 44.9	p= 0.318	N/D
14: apical septal	R= 0.323	**p= 0.022**	979.0 ± 33.4 vs 1020.5 ± 40.5	**p<.001**	N/D
15: apical inferior	R= 0.250	p= 0.086	973.3 ± 36.4 vs 1005.5 ± 51.7	**p= 0.011**	N/D
16: apical lateral	R= 0.070	p= 0.635	981.8 ± 29.4 vs 1004.1 ± 51.3	**p= 0.041**	N/D
global	R= 0.279	**p= 0.050**	983.8 ± 20.5 vs 1002.5 ± 23.9	**p= 0.004**	N/D

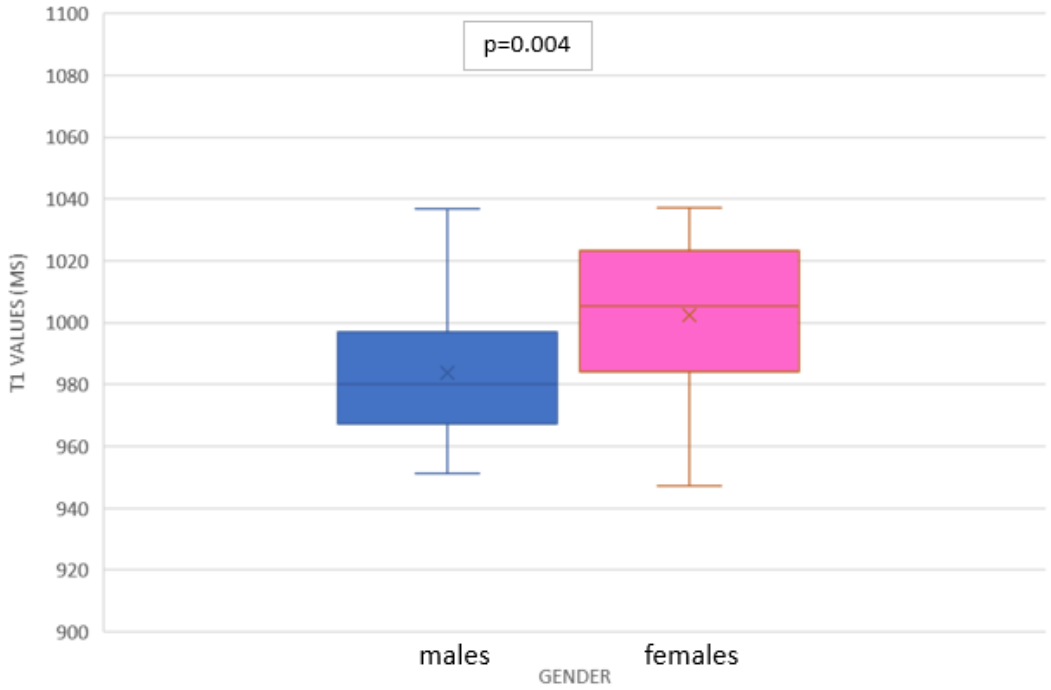

Figure 14: comparison of global T1 values between males and females.

5. T1 VALUES AND CARDIAC CYCLE PHASES

In forty-five patients T1 mapping was acquired both in telediastole and telesystole.

The comparison between T1 mapping obtained in the telediastolic and telesystolic phases showed a statistically significant difference (p= 0.038) (Table V). When analysing the segments, a statistically significant difference was found in the basal anterior and distal septal segments (p=0.003 and p=0.029, respectively).

The ICC value, calculated for individual segments and globally, ranges from a low to an excellent level of intra-class correlation.(Bunting et al., 2019)

Table V: concordance of T1 measurements in telesystole and telediastole

Segment	test for paired data		ICC
	mean difference	P value	
1: basal anterior	-21.1 ± 26.0	**0.003**	0.49
2: basal antero-septal	-4.6 ± 29.4	0.317	0.66
3: basal infero-septal	6.0 ± 17.3	0.219	0.76
4: basal inferior	-6.6 ± 31.9	0.503	0.46
5: basal infero-lateral	-14.7 ± 31.2	0.099	0.52
6: basal antero-lateral	-0.5 ± 23.7	0.298	0.73
7: mid-ventricular anterior	-12.9 ± 31.6	0.103	0.56
8: mid-ventricular antero-septal	0.5 ± 18.0	0.912	0.83
9: mid-ventricular infero-septal	5.4 ± 14.3	0.667	0.84
10: mid-ventricular inferior	-1.5 ± 19.4	0.818	0.72
11: mid-ventricular infero-lateral	-7.1 ± 25.7	0.147	0.56
12: mid-ventricular antero-lateral	-4.6 ± 26.6	0.142	0.65
13: apical anterior	11.0 ± 37.9	0.535	0.58
14: apical septal	13.0 ± 26.7	**0.029**	0.70
15: apical inferior	-8.5 ± 36.4	0.741	0.57
16: apical lateral	-0.7 ± 40.9	0.555	0.32
global	-2.7 ± 11.7	**0.038**	0.87

6. DIASTOLIC REFERENCE VALUES

The average values of T1, relative standard deviations, and corresponding upper and lower limits of normality for global values and all 16 myocardial segments are shown in figures 15-16, for females and males subjects respectively, of all age groups, and in tables VI-VII, for females and males subjects respectively, also stratified by age group.

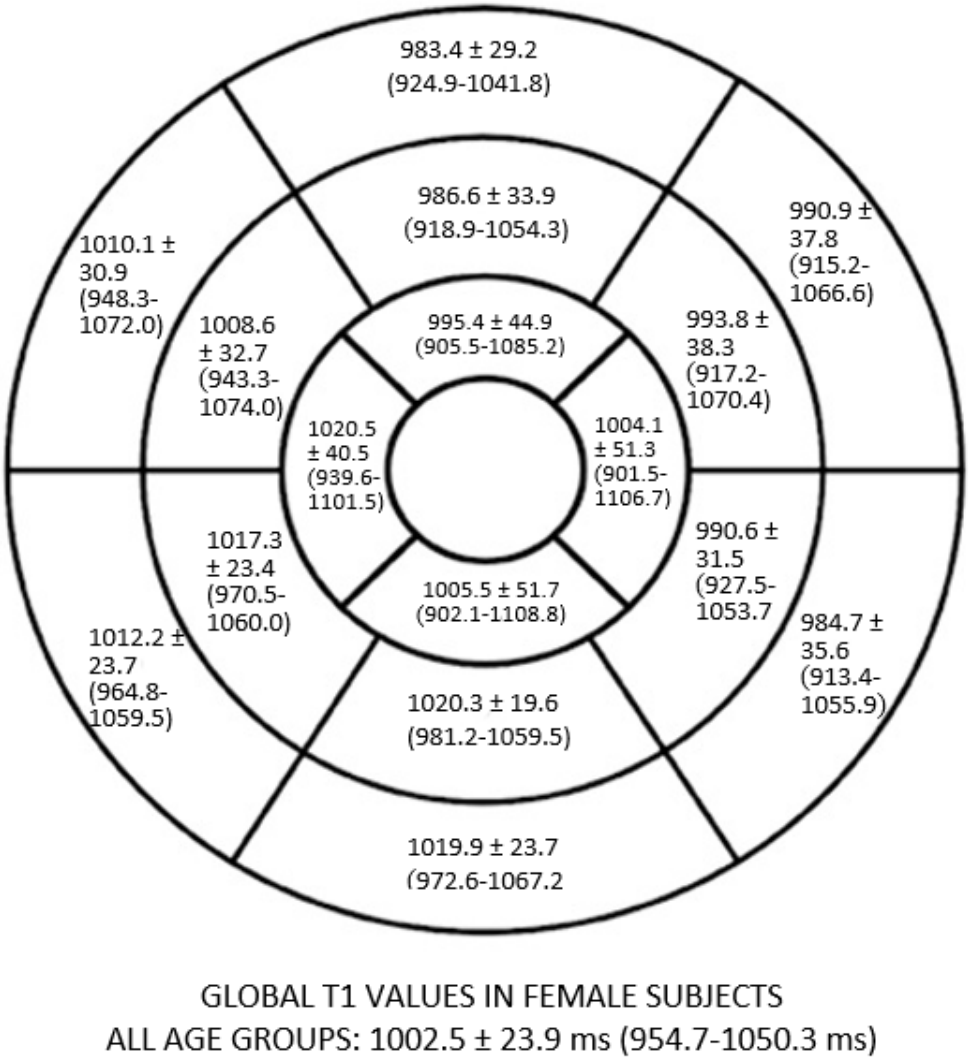

Figure 15: Bull's-eye plots of segmental myocardial T1 values for female subjects. For each segment, the average ± SD and lower and upper limits of normal are displayed.

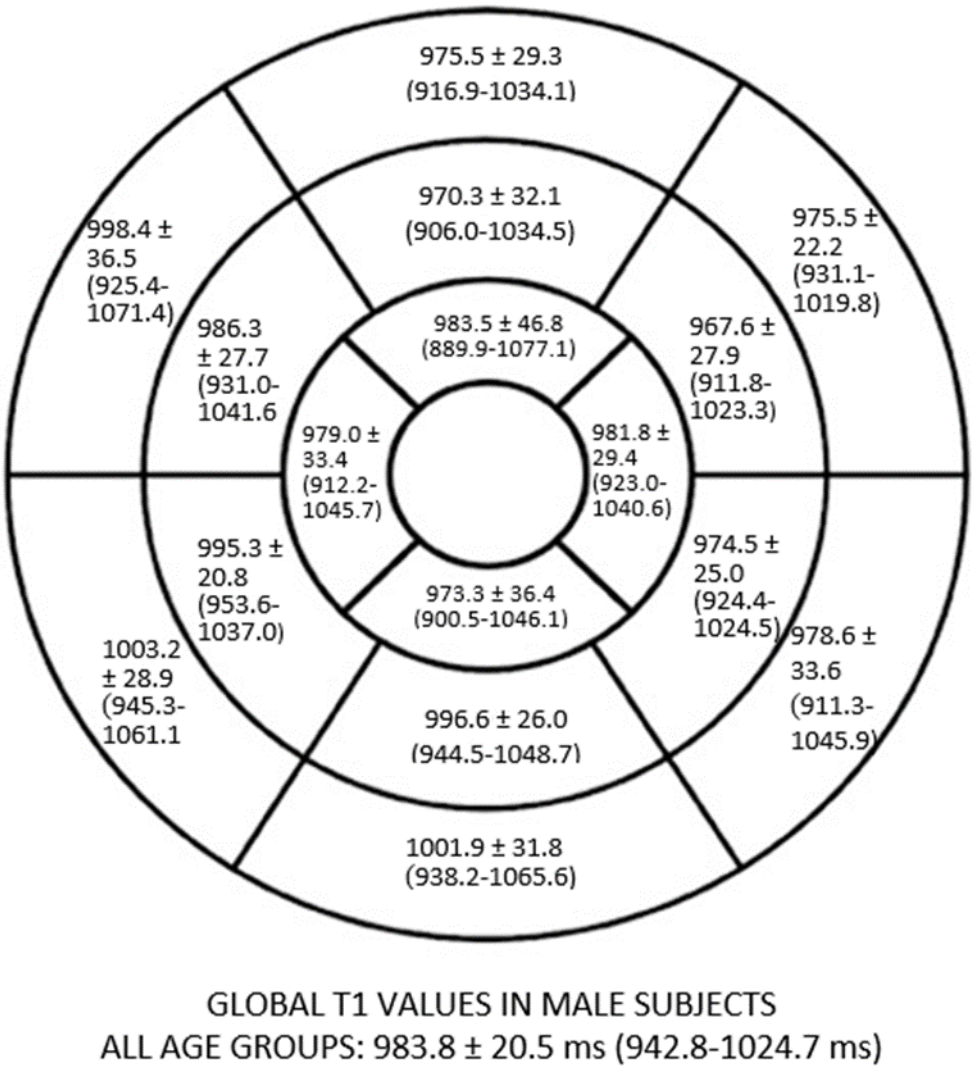

Figure 16: Bull's-eye plots of segmental myocardial T1 values for male subjects. Average ± SD and lower and upper limits of normal are shown for each segment.

Table VI: segmental and global T1 values are tabulated for female subjects stratified by age group; the upper and lower limit values are shown in blue.

T1 VALUES IN FEMALE SUBJECTS

All age groups (ms)		
1: basal anterior	**983.4 ± 29.2**	(924.9-1041.8)
2: basal antero-septal	**1010.1 ± 30.9**	(948.3-1072.0)
3: basal infero-septal	**1012.2 ± 23.7**	(964.8-1059.5)
4: basal inferior	**1019.9 ± 23.7**	(972.6-1067.2)
5: basal infero-lateral	**984.7 ± 35.6**	(913.4-1055.9)
6: basal antero-lateral	**990.9 ± 37.8**	(915.2-1066.6)
7: mid-ventricular anterior	**986.6 ± 33.9**	(918.9-1054.3)
8: mid-ventricular antero-septal	**1008.6 ± 32.7**	(943.3-1074.0)
9: mid-ventricular infero-septal	**1017.3 ± 23.4**	(970.5-1064.0)
10: mid-ventricular inferior	**1020.3 ± 19.6**	(981.2-1059.5)
11: mid-ventricular infero-lateral	**990.6 ± 31.5**	(927.5-1053.7)
12: mid-ventricular antero-lateral	**993.8 ± 38.3**	(917.2-1070.4)
13: apical anterior	**995.4 ± 44.9**	(905.5-1085.2)
14: apical septal	**1020.5 ± 40.5**	(939.6-1101.5)
15: apical inferior	**1005.5 ± 51.7**	(902.1-1108.8)
16: apical lateral	**1004.1 ± 51.3**	(901.5-1106.7)
global	**1002.5 ± 23.9**	(954.7-1050.3)

Age group 20-29 (ms)		
1: basal anterior	**1001.2 ± 18.0**	(965.2-1037.2)
2: basal antero-septal	**1034.2 ± 20.3**	(993.6-1074.8)
3: basal infero-septal	**1028.7 ± 20.9**	(987.0-1070.5)
4: basal inferior	**1025.3 ± 12.5**	(1000.3-1050.3)
5: basal infero-lateral	**999.2 ± 25.1**	(949.0-1049.3)
6: basal antero-lateral	**1002.4 ± 10.4**	(981.6-1023.1)
7: mid-ventricular anterior	**1013.4 ± 27.1**	(959.1-1067.7)
8: mid-ventricular antero-septal	**1029.4 ± 16.8**	(995.7-1063.0)
9: mid-ventricular infero-septal	**1030.0 ± 19.4**	(991.1-1068.9)
10: mid-ventricular inferior	**1030.8 ± 16.8**	(997.2-1064.4)
11: mid-ventricular infero-lateral	**1005.8 ± 19.5**	(966.7-1044.8)
12: mid-ventricular antero-lateral	**1009.4 ± 21.0**	(967.4-1051.5)
13: apical anterior	**1011.1 ± 41.9**	(927.4-1094.8)
14: apical septal	**1054.8 ± 29.3**	(996.1-1113.4)
15: apical inferior	**1017.5 ± 36.0**	(945.5-1089.5)
16: apical lateral	**1033.3 ± 50.5**	(932.2-1134.3)
global	**1020.4 ± 13.1**	(994.2-1046.6)

Age group 30-39 (ms)		
1: basal anterior	**980.1 ± 17.1**	(946.0-1014.2)
2: basal antero-septal	**1002.0 ± 24.0**	(953.9-1050.0)
3: basal infero-septal	**1000.8 ± 19.6**	(961.6.0-1040.1)
4: basal inferior	**1011.4 ± 15.7**	(980.0-1042.7)
5: basal infero-lateral	**991.3 ± 31.9**	(927.4-1055.2)
6: basal antero-lateral	**989.2 ± 28.4**	(932.4-1046.0)
7: mid-ventricular anterior	**979.2 ± 42.6**	(893.9-1064.4)
8: mid-ventricular antero-septal	**1010.0 ± 19.6**	(970.7-1049.3)
9: mid-ventricular infero-septal	**1001.2 ± 22.4**	(956.4-1045.9)
10: mid-ventricular inferior	**1008.3 ± 21.8**	(964.6-1052.0)
11: mid-ventricular infero-lateral	**987.5 ± 34.1**	(919.4-1055.7)
12: mid-ventricular antero-lateral	**980.3 ± 22.6**	(935.2-1025.5)
13: apical anterior	**992.6 ± 62.4**	(867.7-1117.4)
14: apical septal	**1025.7 ± 37.1**	(951.5-1100.0)
15: apical inferior	**1019.9 ± 43.7**	(932.5-1107.2)
16: apical lateral	**1007.4 ± 47.0**	(913.4-1101.4)
global	**998.4 ± 22.7**	(952.9-1043.8)

Age group 40-49 (ms)		
1: basal anterior	**978.1 ± 26.5**	(925.2-1031.0)
2: basal antero-septal	**1023.6 ± 37.3**	(949.0-1098.2)
3: basal infero-septal	**1025.3 ± 12.8**	(999.8-1050.8)
4: basal inferior	**1032.9 ± 23.8**	(985.4-1080.4)
5: basal infero-lateral	**985.9 ± 31.7**	(922.4-1049.3)
6: basal antero-lateral	**1016.9 ± 46.4**	(924.2-1109.6)
7: mid-ventricular anterior	**998.9 ± 23.3**	(952.3-1045.4)
8: mid-ventricular antero-septal	**1029.7 ± 39.0**	(951.7-1107.7)
9: mid-ventricular infero-septal	**1036.8 ± 10.5**	(1015.7-1057.9)
10: mid-ventricular inferior	**1027.5 ± 12.0**	(1003.6-1051.5)
11: mid-ventricular infero-lateral	**1005.0 ± 16.6**	(971.8-1038.1)
12: mid-ventricular antero-lateral	**1021.4 ± 44.5**	(932.4-1110.5)
13: apical anterior	**986.4 ± 43.9**	(898.5-1074.3)
14: apical septal	**1019.8 ± 29.8**	(960.2-1079.4)
15: apical inferior	**1000.2 ± 52.9**	(894.4-1105.9)
16: apical lateral	**986.8 ± 57.2**	(872.5-1101.2)
global	**1011.4 ± 18.3**	(974.8-1048.0)

Age group 50-59 (ms)		
1: basal anterior	**981.2 ± 43.3**	(894.7-1067.7)
2: basal antero-septal	**991.5 ± 37.1**	(917.4-1065.7)
3: basal infero-septal	**1004.1 ± 29.9**	(944.3-1064.0)
4: basal inferior	**1021.0 ± 17.7**	(985.7-1056.3)
5: basal infero-lateral	**966.5 ± 51.7**	(863.1-1069.8)
6: basal antero-lateral	**972.8 ± 51.9**	(868.9-1076.7)
7: mid-ventricular anterior	**973.5 ± 35.5**	(902.5-1044.5)
8: mid-ventricular antero-septal	**985.1 ± 42.3**	(900.5-1069.7)
9: mid-ventricular infero-septal	**1007.5 ± 29.1**	(949.4-1065.6)
10: mid-ventricular inferior	**1017.4 ± 16.4**	(984.6-1050.3)
11: mid-ventricular infero-lateral	**972.8 ± 39.0**	(894.7-1050.8)
12: mid-ventricular antero-lateral	**979.0 ± 43.1**	(892.8-1065.3)
13: apical anterior	**993.0 ± 45.7**	(901.5-1084.4)
14: apical septal	**1002.4 ± 59.8**	(882.9-1121.9)
15: apical inferior	**1038.2 ± 41.1**	(956.0-1120.4)
16: apical lateral	**1008.2 ± 49.3**	(909.7-1106.8)
global	**993.5 ± 35.5**	(922.5-1064.6)

Age group 60-69 (ms)		
1: basal anterior	**976.2 ± 37.7**	(900.8-1051.7)
2: basal antero-septal	**999.3 ± 19.2**	(960.9-1037.8)
3: basal infero-septal	**1001.8 ± 23.6**	(954.6-1049.1)
4: basal inferior	**1008.8 ± 39.8**	(929.2-1088.5)
5: basal infero-lateral	**980.5 ± 39.2**	(902.1-1058.9)
6: basal antero-lateral	**973.2 ± 31.8**	(909.5-1036.9)
7: mid-ventricular anterior	**967.8 ± 26.5**	(914.7-1020.9)
8: mid-ventricular antero-septal	**988.9 ± 12.5**	(963.9-1013.9)
9: mid-ventricular infero-septal	**1010.9 ± 16.4**	(978.1-1043.7)
10: mid-ventricular inferior	**1017.5 ± 26.9**	(963.7-1071.3)
11: mid-ventricular infero-lateral	**982.0 ± 39.8**	(902.5-1061.5)
12: mid-ventricular antero-lateral	**978.7 ± 44.2**	(890.2-1067.1)
13: apical anterior	**992.0 ± 44.6**	(902.8-1081.2)
14: apical septal	**1000.1 ± 26.4**	(947.3-1052.8)
15: apical inferior	**961.0 ± 62.7**	(835.6-1086.4)
16: apical lateral	**980.8 ± 58.5**	(863.8-1097.7)
global	**989.0 ± 17.1**	(954.9-1023.2)

table V: Segmental and global T1 values tabulated for female subjects by age group; in blue the upper and lower limit values

Table VII: segmental and global T1 values are tabulated for male subjects stratified by age group; the upper and lower limit values are shown in blue.

T1 VALUES IN MALE SUBJECTS

All age groups (ms)		
1: basal anterior	**975.5 ± 29.3**	**(916.9-1034.1)**
2: basal antero-septal	**998.4 ± 36.5**	**(925.4-1071.4)**
3: basal infero-septal	**1003.2 ± 28.9**	**(945.3-1061.1)**
4: basal inferior	**1001.9 ± 31.8**	**(938.2-1065.6)**
5: basal infero-lateral	**978.6 ± 33.6**	**(911.3-1045.9)**
6: basal antero-lateral	**975.5 ± 22.2**	**(931.1-1019.8)**
7: mid-ventricular anterior	**970.3 ± 32.1**	**(906.0-1034.5)**
8: mid-ventricular antero-septal	**986.3 ± 27.7**	**(931.0-1041.6)**
9: mid-ventricular infero-septal	**995.3 ± 20.8**	**(953.6-1037.0)**
10: mid-ventricular inferior	**996.6 ± 26.0**	**(944.5-1048.7)**
11: mid-ventricular infero-lateral	**974.5 ± 25.0**	**(924.4-1024.5)**
12: mid-ventricular antero-lateral	**967.6 ± 27.9**	**(911.8-1023.3)**
13: apical anterior	**983.5 ± 46.8**	**(889.9-1077.1)**
14: apical septal	**979.0 ± 33.4**	**(912.2-1045.7)**
15: apical inferior	**973.3 ± 36.4**	**(900.5-1046.1)**
16: apical lateral	**981.8 ± 29.4**	**(923.0-1040.6)**
global	**983.8 ± 20.5**	**(942.8-1024.7)**

Age group 20-29 (ms)		
1: basal anterior	**985.0 ± 28.2**	**(928.7-1041.3)**
2: basal antero-septal	**1009.2 ± 32.8**	**(943.6-1074.8)**
3: basal infero-septal	**1015.1 ± 33.9**	**(947.3-1082.9)**
4: basal inferior	**997.5 ± 34.0**	**(929.5-1065.6)**
5: basal infero-lateral	**985.9 ± 28.2**	**(929.5-1042.3)**
6: basal antero-lateral	**970.0 ± 19.1**	**(931.8-1008.2)**
7: mid-ventricular anterior	**990.1 ± 47.8**	**(894.5-1085.6)**
8: mid-ventricular antero-septal	**1007.9 ± 27.0**	**(953.9-1061.8)**
9: mid-ventricular infero-septal	**1006.1 ± 20.8**	**(964.5-1047.7)**
10: mid-ventricular inferior	**1004.2 ± 29.3**	**(945.5-1062.9)**
11: mid-ventricular infero-lateral	**980.7 ± 22.6**	**(935.6-1025.9)**
12: mid-ventricular antero-lateral	**965.2 ± 31.4**	**(902.3-1028.0)**
13: apical anterior	**1004.2 ± 55.7**	**(892.8-1115.5)**
14: apical septal	**1003.2 ± 24.8**	**(953.5-1052.9)**
15: apical inferior	**994.9 ± 31.7**	**(931.5-1058.3)**
16: apical lateral	**988.4 ± 32.0**	**(924.4-1052.5)**
global	**994.2 ± 28.2**	**(937.7-1050.7)**

Age group 30-39 (ms)		
1: basal anterior	**982.7 ± 38.1**	**(906.6-1058.8)**
2: basal antero-septal	**1013.1 ± 43.3**	**(926.6-1099.6)**
3: basal infero-septal	**1010.1 ± 23.9**	**(962.2-1057.9)**
4: basal inferior	**996.6 ± 33.1**	**(930.4-1062.8)**
5: basal infero-lateral	**973.4 ± 23.0**	**(927.5-1019.3)**
6: basal antero-lateral	**970.5 ± 23.1**	**(924.3-1016.8)**
7: mid-ventricular anterior	**971.0 ± 20.1**	**(930.8-1011.2)**
8: mid-ventricular antero-septal	**991.3 ± 24.1**	**(943.0-1039.6)**
9: mid-ventricular infero-septal	**998.8 ± 13.7**	**(971.3-1026.2)**
10: mid-ventricular inferior	**985.0 ± 16.2**	**(952.6-1017.3)**
11: mid-ventricular infero-lateral	**969.2 ± 18.7**	**(931.7-1006.7)**
12: mid-ventricular antero-lateral	**961.3 ± 16.8**	**(927.6-994.9)**
13: apical anterior	**988.6 ± 45.8**	**(897.1-1080.1)**
14: apical septal	**984.5 ± 44.3**	**(895.9-1073.1)**
15: apical inferior	**975.9 ± 21.4**	**(933.1-1018.7)**
16: apical lateral	**961.2 ± 24.8**	**(911.7-1010.8)**
global	**983.3 ± 19.3**	**(944.7-1022.0)**

Age group 40-49 (ms)		
1: basal anterior	**970.2 ± 26.7**	**(916.8-1023.6)**
2: basal antero-septal	**981.0 ± 30.9**	**(919.3-1042.7)**
3: basal infero-septal	**990.2 ± 18.1**	**(953.9-1026.4)**
4: basal inferior	**1006.0 ± 35.9**	**(934.1-1077.9)**
5: basal infero-lateral	**975.4 ± 31.8**	**(911.8-1038.9)**
6: basal antero-lateral	**969.9 ± 28.4**	**(913.1-1026.8)**
7: mid-ventricular anterior	**965.8 ± 34.2**	**(897.4-1034.1)**
8: mid-ventricular antero-septal	**974.0 ± 30.9**	**(912.2-1035.9)**
9: mid-ventricular infero-septal	**990.1 ± 18.3**	**(953.5-1026.6)**
10: mid-ventricular inferior	**988.2 ± 27.5**	**(933.2-1043.3)**
11: mid-ventricular infero-lateral	**983.9 ± 29.6**	**(924.7-1043.1)**
12: mid-ventricular antero-lateral	**968.6 ± 39.9**	**(888.9-1048.4)**
13: apical anterior	**968.6 ± 67.5**	**(833.5-1103.6)**
14: apical septal	**948.7 ± 27.6**	**(893.6-1003.8)**
15: apical inferior	**951.5 ± 33.2**	**(885.0-1018.0)**
16: apical lateral	**977.3 ± 33.0**	**(911.3-1043.4)**
global	**975.6 ± 19.8**	**(935.9-1015.3)**

Age group 50-59 (ms)		
1: basal anterior	**963.7 ± 27.4**	**(908.9-1018.4)**
2: basal antero-septal	**986.3 ± 44.1**	**(898.0-1074.5)**
3: basal infero-septal	**997.3 ±25.5**	**(946.2-1048.4)**
4: basal inferior	**1001.6 ± 17.5**	**(966.6-1036.5)**
5: basal infero-lateral	**992.0 ± 30.6**	**(930.7-1053.2)**
6: basal antero-lateral	**974.6 ± 19.6**	**(935.3-1013.8)**
7: mid-ventricular anterior	**981.2 ± 17.6**	**(945.9-1016.4)**
8: mid-ventricular antero-septal	**970.9 ± 28.4**	**(914.0-1027.8)**
9: mid-ventricular infero-septal	**987.2 ± 22.1**	**(943.0-1031.4)**
10: mid-ventricular inferior	**995.4 ± 11.6**	**(972.1-1018.7)**
11: mid-ventricular infero-lateral	**972.8 ± 36.1**	**(900.5-1045.0)**
12: mid-ventricular antero-lateral	**974.6 ± 14.3**	**(946.0-1003.2)**
13: apical anterior	**991.5 ± 28.2**	**(935.1-1047.8)**
14: apical septal	**975.1 ± 29.4**	**(916.3-1033.9)**
15: apical inferior	**957.2 ± 30.8**	**(895.6-1018.8)**
16: apical lateral	**984.0 ± 29.8**	**(924.5-1043.5)**
global	**981.6 ± 19.9**	**(941.8-1021.3)**

Age group 60-69 (ms)		
1: basal anterior	**975.7 ± 32.6**	**(910.6-1040.8)**
2: basal antero-septal	**1002.2 ± 33.9**	**(934.5-1070.0)**
3: basal infero-septal	**1003.3 ± 42.8**	**(917.7-1088.9)**
4: basal inferior	**1008.0 ± 45.9**	**(916.1-1099.9)**
5: basal infero-lateral	**966.2 ± 54.7**	**(856.8-1075.7)**
6: basal antero-lateral	**992.3 ± 20.0**	**(952.2-1032.4)**
7: mid-ventricular anterior	**943.5 ± 21.6**	**(900.3-986.6)**
8: mid-ventricular antero-septal	**987.3 ± 20.4**	**(946.4-1028.1)**
9: mid-ventricular infero-septal	**994.1 ± 29.8**	**(934.6-1053.6)**
10: mid-ventricular inferior	**1013.7 ± 41.0**	**(931.7-1095.6)**
11: mid-ventricular infero-lateral	**963.4 ± 18.0**	**(927.4-999.4)**
12: mid-ventricular antero-lateral	**968.2 ± 38.2**	**(891.3-1045.0)**
13: apical anterior	**964.8 ± 35.3**	**(894.2-1035.5)**
14: apical septal	**983.3 ± 22.8**	**(937.7-1028.8)**
15: apical inferior	**987.0 ± 51.9**	**(883.2-1090.8)**
16: apical lateral	**998.0 ± 25.1**	**(947.9-1048.1)**
global	**984.2 ± 18.1**	**(948.0-1020.4)**

table IV: Segmental and global T1 values tabulated for male subjects by age group; in blue the upper and lower normality limits

7. CLINICAL APPLICATIONS

Examples of clinical relevance in applying the reference values obtained in our own Institute, compared to literature values, are reported below.

7.1 CASE 1

Male patient, 51 years old, affected by systemic sclerosis with diffuse scleroderma. He underwent CMR for a recent Covid pneumonia and the suspicion of myocarditis. Before Covid-19 infection his cardiovascular history was negative.

The global T1 value was 1034 ms, normal according to the literature (855-1039 ms) (Piechnik et al., 2010), but high according to our normal cut off values for his sex and age (n.r. 941.8-1021.3 ms). [Figure 17]

Also considering the T2 values, the MRI findings were compatible with acute/subacute myocarditis. Moreover, at the segmental level the matching between high T2 and high T1 values was higher using the cut off of our Institute.

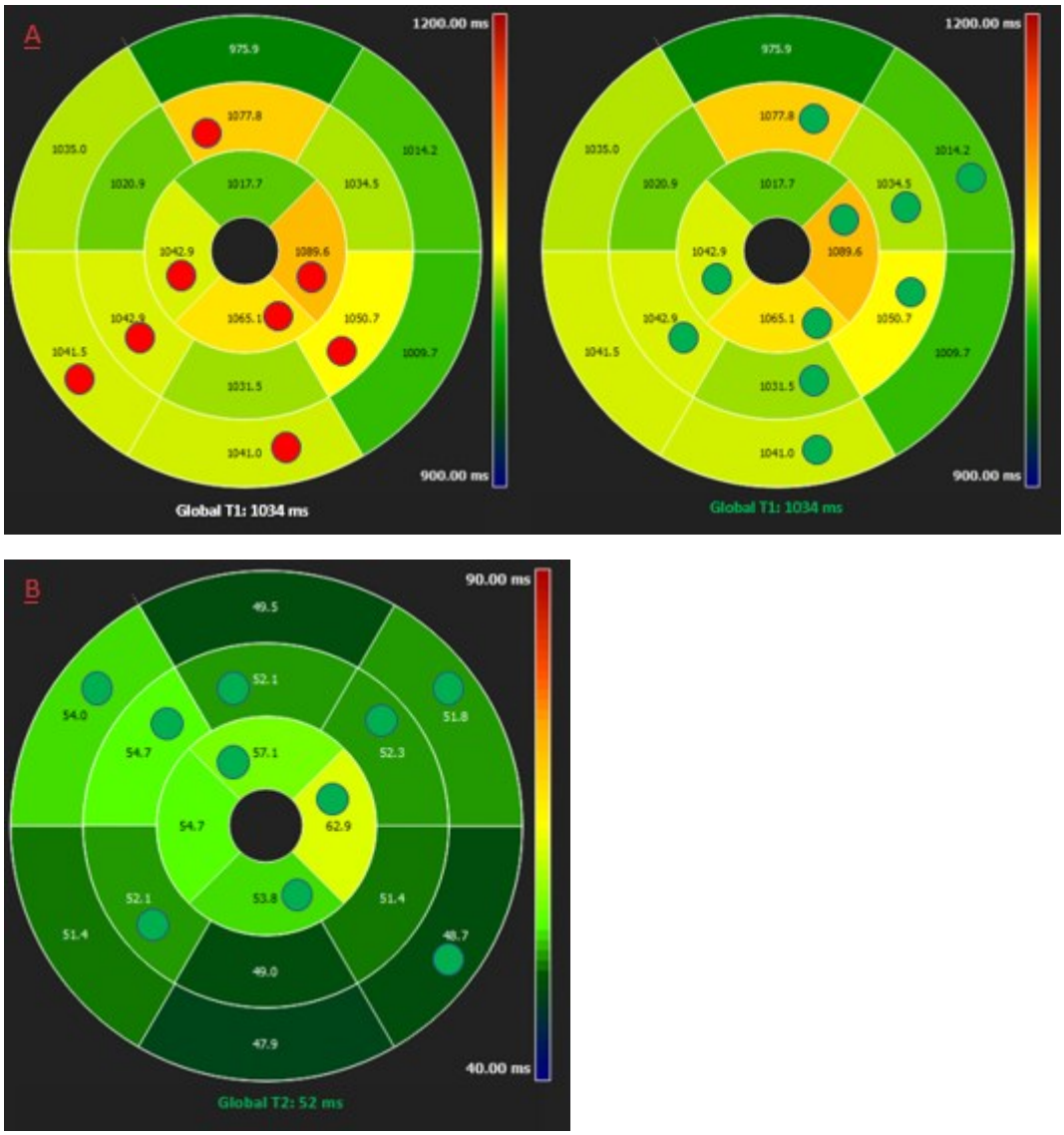

Figure 18: A T1 map of patient 1. Red circles show segments with high T1 values following the normal reference values from the literature. Green circles show the segments with high T1 values based on the normal cut off for our Institute. B T2 map of patient 1. Green circles show the segments with high T2 values based on the normal cut off for our Institute

7.2. CASE 2

Female patient, 55 years old, underwent CMR for palpitations and for a left global systolic function at lower limit, septal hypokinesis and mild mitral regurgitation by echocardiography.

The patient had high T1 values in basal inferior and infero-septal, and distal lateral segments if considering the literature (i.e., T1≥1040 ms), but normal ones considering our ranges for her age (n.r. 922.5-1064.6 ms). [Figure 18] Consequently, as regards T1 values, no pathological values were found.

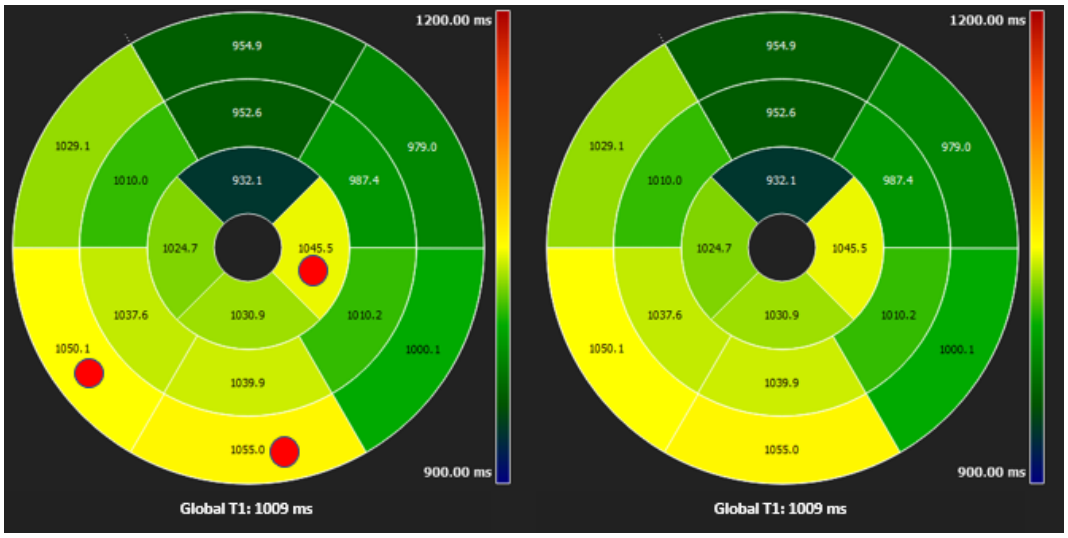

Figure 18: T1 map of patient 3. Red circles show segments with high T1 values following the normal reference values from the literature. No segmental high T1 values were found based on the normal cut off for our Institute.

7.3 CASE 3

Female patient, 19 years old, was underwent CMR for alterations in ventricular repolarisation after Covid-19 infection. The global T1 value (977 ms) resulted decreased following the normal reference cut off values for our Institute (n.r. 994.2-1046.6 ms), as well as for four segmental T1 values [Figure 19]. Following the reference values from the literature (855-1039 ms) (Piechnik et al., 2010) global and segmental T1 values were normal with the exception for the lateral distal segment. Based on the CMR report, using the specific normal cut off from our Institute, the patient was referred to the clinician with the suspicion for hemochromatosis or for Anderson-Fabry disease.

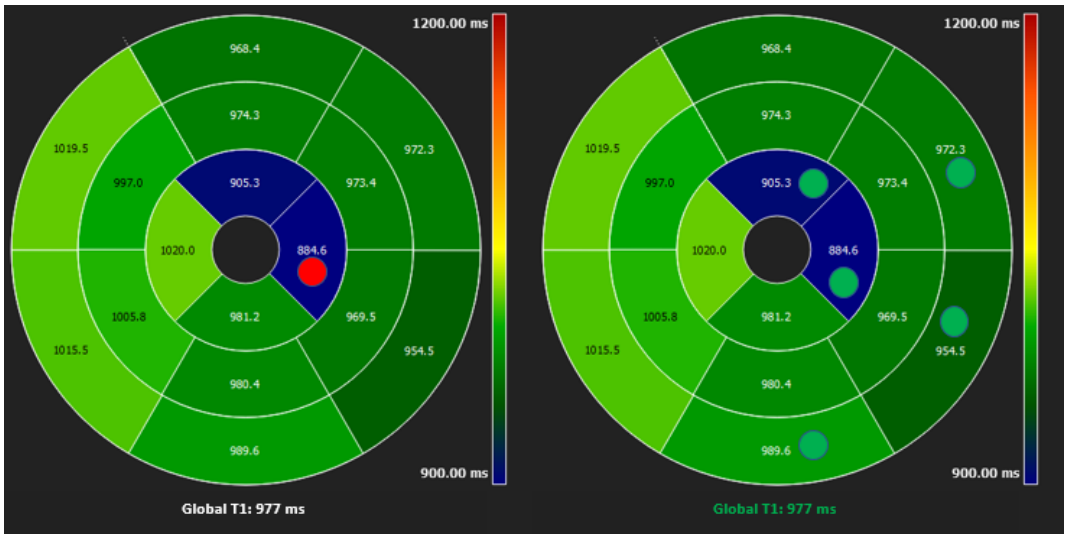

Figure 19: T1 map for the patient 4. Red circles show segments with high T1 values following the normal reference values from the literature. Green circles show segments with low T1 values following the normal cut off of our Institute.

DISCUSSION

The use of T1 mapping allows a non-invasive myocardial tissue characterization, obtaining a series of quantitative values that are useful for an accurate and tailored clinical management of the patients. It finds application in detecting the presence of fibrosis, amyloid, iron, fat, resulting very useful in the diagnosis of ischemia, inflammation, amyloidosis, hemochromatosis, Anderson-Fabry disease, and all other pathological condition characterized by altered T1 values.

As known, these values strongly depend on the type of sequence and the scanner used, as encoded in international consensus documents (Messroghli, 2017), and it is furthermore essential, for clinical use, to know the variations in T1 mapping values with respect to physiological parameters, such as age and gender.

For these reasons, every centre should obtain its own reference values from a consistent number of healthy subjects.

The purpose of this study was to acquire native T1 values and observe the possible physiological variations which are due to gender, age, and cardiac cycle phase, in a population of healthy volunteers, using a Siemens 1.5 T scanner, MOLLI sequences and the commercially available software (cvi42).

The meticulous selection of the subjects, stratified by age and sex, and with strict inclusion criteria, allowed us to obtain robust results.

To the best of our knowledge, this is the first study that evaluate 16 segmental and global T1 normal values with a 1.5 T Siemens scanner, using MOLLI sequences analysed with cvi42 software in a large study population stratified for sex and age. In the literature, there was only one previous study that used three slices (Piechnik et al., 2010), on a smaller and unbalanced population (n=10, 7 males and 3 females).

1. REPEATABILITY

Our study provides evidence for good intra-observer, inter-observer, and inter-study repeatability.

The reproducibility analysis carried out showed excellent intra-class correlation of the overall values (ICC ≥ 0.80 in all); this testifies to the high agreement of the T1 values obtained between the various measurements, in addition to the absence of systematic bias caused by the repetition of the study and by different intra- and inter-operator observations [Figure 5]. In this way the T1 mapping techniques is confirmed to be robust and highly reproducible. The high reproducibility gives confidence that changes in T1 values in clinical practice may reflect specific tissue characteristics.

Most of the T1 maps acquired in diastole were adequate; only 0.875% of the total segments had to be excluded from the analysis due to artifacts and were mostly in the distal section, probably due to the partial volume effect for the thin wall.

2. CORRELATIONS BETWEEN THE VALUES OF T1 MAPPING AND THE POPULATION CHARACTERISTICS

The effect of the population's characteristics on T1 values was evaluated, focusing on age differences, gender, wall thickness, and phase of the cardiac cycle. It is important to know the variations of T1 values according to these parameters to distinguish the pathological values from the normal ones.

In our study, the global native T1 value averaged at 993.2 ± 24.0 (range = 945.2-1041.2 ms) considering all subjects. Our results differ from the normal values of Rosmini et al (Rosmini et al., 2018) (1025 ± 38 ms), obtained with a 1.5 T MAGNETOM Avanto Siemens scanner, using the same MOLLI sequences 5(3)3 and the same flip angle. However, they acquired only a mid-ventricular short axis slice. That study was carried out with a larger sample (i.e., ninety-four healthy volunteers), with a significantly higher mean age than the one in our study population (50 ± 14 vs 43.2 ± 13.9 years) (p=0.006). Moreover, it had a slightly unbalanced gender distribution (52% males) but a different ethnicity distribution, with Caucasian, Asian, black/Afro-Caribbean, and other minor ethnicities represented.

Our normal T1 values differed also from the ones found by Piechnick (Piechnik et al., 2010) that it is the unique study with our same methodology (Siemens 1.5 T, end-expiration basal, mid-cavity and distal short-axis slices using MOLLI analysed by cvi42). However, the study from Piechnick et al was strongly limited by the small number of volunteers no stratified for sex and age: 10 normal volunteers (7 men), with a different age (35 ± 7 years).

As expected, our normal values also differed from those obtained with a 1.5 T from other vendors: Philips scanner in Dabir et al study (950 ± 21 ms, range 908-992 ms) (Dabir et al., 2014) , General Electric scanner in Meloni et a study (1015 ± 37 ms, range 932-1112)l (Meloni, et al., 2021)

Both the Dabir et al. (Dabir et al., 2014), and Meloni et al. (Meloni, et al., 2021) studies enrolled a larger number of healthy volunteers (102 and 100, respectively), with a wider age range in Dabir et al. (17-83) and a gender distribution of 53 males and 49 females, while Meloni et al. had the same age range as our study (20-69) and the same gender distribution.

The difference is probably attributable primarily to the different vendors and design of the sequence, secondary to the different sample size, with subject of different mean age.

This data confirms the need for each single centre to have specific T1 normative values, as recommended by the international literature (Messroghli 2017).

In our study, we found a statistically significant difference in T1 global values among gender, with lower values in males, and among the mid-ventricular and distal segments in males and females, as confirmed by other studies (Rosmini et al., 2018) (Meloni, et al., 2021) (Dabir et al., 2014). As regards the basal segments, unlike in the previous studies, no statistically significant difference was found between the two genders.

Longer T1 values in females may be explained by a higher proclivity to partial-volume effects due to thinner myocardium (Tessa et al., 2015), higher blood T1 values due to lower haematocrit values or different tissue characteristics due to hormone status (Regitz-Zagrosek, 2006). There is the possibility of research into

understanding whether sex hormone status may influence myocardial tissue characteristics as reflected by myocardial native T1, since oestrogen, progesterone, and androgens have effects on myocardial structure and function. (Rauhalammi et al., 2016) Thus, our results confirm the need to use different normality reference values between male and female subjects.

Globally, in our study there were no significant statistical differences between myocardial sections, as found by in Tessa et al. (Tessa et al., 2015) using our same methodology, with the exception for the software of analysis, in a smaller population no stratified for sex and age; considering males only, the comparison between basal and mid-ventricular sections showed a significant difference, with lower values in the latter (p=0.01). Conversely, Meloni et al. (Meloni, et al., 2021), found significantly lower values in the basal slice compared with both medial and distal ones, probably due to more partial volume artefacts using GE scanners.

A weak positive statistical correlation (p=0.050) between patient age and T1 values was found in our population, while Rosmini observed that native T1 was slightly lower with age. (Rosmini et al., 2018) . Conversely, in Meloni et al native T1 values were not associated with age. These discrepancies probably reflect the differences in the enrolled population among the studies.

According with other studies (Meloni, et al., 2021) there was a significant difference between males and females left ventricular wall thickness, with higher values in the male subjects. However, no significant statistical correlation between wall thickness and native global and segmental T1 values was found in our study supporting the hypothesis of less partial volume artefacts using Siemens scanners.

An important difference emerges from the analysis of the T1 values in end systole and end diastole, with lower values in the systolic phase of the cardiac cycle (p=0.038; ICC=0.87). Global T1 values were higher in diastole than in systole also in other studies (Meloni, et al., 2021) (Kawel et al., 2012) (Reiter et al., 2014)and are likely to be related to physiologic variations in myocardial blood volume during the cardiac cycle. (Wu et al., 2004) Furthermore, a relationship with the different characteristics of the myocardium in the different phases of the cardiac cycle cannot be excluded. In any case, this difference between systole and diastole

suggests a standardization of the study protocol in the end-diastolic or end-systolic phase and, to avoid potential bias, it is recommended that T1 measurements be obtained during the same cardiac phase.(Tessa et al., 2015) In clinical practice, to date, it is preferable to acquire T1 mapping images in the end diastolic phase, because they are less sensitive to movement artifacts; however, compared to the end systolic phase, they are more susceptible to partial volume artifacts, in particular in the distal sections (Messroghli 2017).

3. CLINICAL APPLICATIONS

In applying the reference values obtained in our own Institute, compared to literature values, we showed the importance of sex and age specific normal cut off values for the diagnosis of health versus disease avoiding misclassifications.

LIMITATIONS

This was a single centre study evaluating only one mapping sequence (MOLLI) with one dedicated commercially available software package (cvi42) and one specific 1.5 T scanner (Siemens MAGNETOM Avanto).

Multicentre studies are recommended to test the transferability for the T1 mapping methodology.

The T1 values obtained from this study were collected from an exclusively Caucasian population. Therefore, in the future, it will be necessary to conduct other studies to evaluate possible variations in the magnetic properties of the healthy myocardium related to different ethnic groups.

The obtained T1 values refer to an adult population. Further studies aiming to evaluate the normal values of myocardial relaxation times of paediatric patients will need to be conducted.

CONCLUSIONS

Cardiac magnetic resonance mapping is a diagnostic tool that has seen many innovations in the last decade and is likely to continue to develop in the future.

In our experience, MOLLI sequences allow a reliable, robust, and reproducible quantification of global and segmental T1 values.

The differences, identified according to the stage of acquisition, gender, and age for T1 values, suggest the need to implement specific reference values for these variables, to avoid systematic errors in the identification of pathological pictures.

To the best of our knowledge, this is the first study to evaluate 16 segmental and global T1 normal values with a 1.5 T Siemens scanner, using MOLLI sequences analysed with cvi42 software, on a large population stratified for sex and age.

The normality ranges defined in this study, obtained by focusing on the effect of population characteristics, may be used as age- and gender-specific reference values for the Institute of Radiology of the University Hospital of Padua, and likely for other centres using the same scanner, sequence, and software of analysis.

Thus, in clinical practice, robust use of quantitative parametric T1 mapping sequences to characterize myocardial tissue will be possible in order to obtain quantitative, and possibly early, diagnostic information that can improve the prognosis of our patients.

REFERENCES

Banypersad, S. M., Fontana, M., Maestrini, V., Sado, D. M., Captur, G., Petrie, A., Piechnik, S. K., Whelan, C. J., Herrey, A. S., Gillmore, J. D., Lachmann, H. J., Wechalekar, A. D., Hawkins, P. N., & Moon, J. C. (2015). T1 mapping and survival in systemic light-chain amyloidosis. *European Heart Journal*, *36*(4). https://doi.org/10.1093/eurheartj/ehu444

Bordonaro, V., Bivort, D., Dresselaers, T., de Langhe, E., Bogaert, J., & Symons, R. (2021). Myocardial T1 mapping and extracellular volume quantification as novel biomarkers in risk stratification of patients with systemic sclerosis. *Clinical Radiology*, *76*(2). https://doi.org/10.1016/j.crad.2020.09.023

Brosnan, M., & Rakhit, D. (2018). Differentiating Athlete's Heart From Cardiomyopathies — The Left Side. In *Heart Lung and Circulation* (Vol. 27, Issue 9). https://doi.org/10.1016/j.hlc.2018.04.297

Bunting, K. v., Steeds, R. P., Slater, L. T., Rogers, J. K., Gkoutos, G. v., & Kotecha, D. (2019). A Practical Guide to Assess the Reproducibility of Echocardiographic Measurements. In *Journal of the American Society of Echocardiography* (Vol. 32, Issue 12, pp. 1505–1515). Mosby Inc. https://doi.org/10.1016/j.echo.2019.08.015

Carberry, J., Carrick, D., Haig, C., Rauhalammi, S. M., Ahmed, N., Mordi, I., McEntegart, M., Petrie, M. C., Eteiba, H., Hood, S., Watkins, S., Lindsay, M., Davie, A., Mahrous, A., Ford, I., Sattar, N., Welsh, P., Radjenovic, A., Oldroyd, K. G., & Berry, C. (2016). Remote Zone Extracellular Volume and Left Ventricular Remodeling in Survivors of ST-Elevation Myocardial Infarction. *Hypertension*, *68*(2). https://doi.org/10.1161/HYPERTENSIONAHA.116.07222

Carrick, D., Haig, C., Rauhalammi, S., Ahmed, N., Mordi, I., McEntegart, M., Petrie, M. C., Eteiba, H., Hood, S., Watkins, S., Lindsay, M., Mahrous, A., Ford, I., Tzemos, N., Sattar, N., Welsh, P., Radjenovic, A., Oldroyd, K. G., & Berry, C. (2016). Prognostic significance of infarct core pathology revealed by quantitative non-contrast in comparison with contrast cardiac magnetic resonance imaging in reperfused ST-elevation myocardial infarction survivors. *European Heart Journal*, *37*(13). https://doi.org/10.1093/eurheartj/ehv372

Cerqueira, M. D., Weissman, N. J., Dilsizian, V., Jacobs, A. K., Kaul, S., Laskey, W. K., Pennell, D. J., Rumberger, J. A., Ryan, T. J., & Verani, M. S. (2002). Standardized myocardial segmentation and nomenclature for tomographic imaging of the heart. *Journal of Cardiovascular Magnetic Resonance*, *4*(2). https://doi.org/10.1081/JCMR-120003946

Chan, W., Duffy, S. J., White, D. A., Gao, X. M., Du, X. J., Ellims, A. H., Dart, A. M., & Taylor, A. J. (2012). Acute left ventricular remodeling following myocardial infarction: Coupling of regional healing with remote extracellular matrix expansion. *JACC: Cardiovascular Imaging*, *5*(9). https://doi.org/10.1016/j.jcmg.2012.03.015

Dabir, D., Child, N., Kalra, A., Rogers, T., Gebker, R., Jabbour, A., Plein, S., Yu, C. Y., Otton, J., Kidambi, A., McDiarmid, A., Broadbent, D., Higgins, D. M., Schnackenburg, B., Foote, L., Cummins, C., Nagel, E., & Puntmann, V. O. (2014). Reference values for healthy human myocardium using a T1 mapping methodology: results from the

International T1 Multicenter cardiovascular magnetic resonance study. *Journal of Cardiovascular Magnetic Resonance : Official Journal of the Society for Cardiovascular Magnetic Resonance*, *16*, 69. https://doi.org/10.1186/s12968-014-0069-x

Dall'Armellina, E., Piechnik, S. K., Ferreira, V. M., Si, Q. le, Robson, M. D., Francis, J. M., Cuculi, F., Kharbanda, R. K., Banning, A. P., Choudhury, R. P., Karamitsos, T. D., & Neubauer, S. (2012). Cardiovascular magnetic resonance by non contrast T1-mapping allows assessment of severity of injury in acute myocardial infarction. *Journal of Cardiovascular Magnetic Resonance*, *14*(1). https://doi.org/10.1186/1532-429X-14-15

Demirkiran, A., Everaars, H., Amier, R. P., Beijnink, C., Bom, M. J., Götte, M. J. W., van Loon, R. B., Selder, J. L., van Rossum, A. C., & Nijveldt, R. (2019). Cardiovascular magnetic resonance techniques for tissue characterization after acute myocardial injury. In *European Heart Journal Cardiovascular Imaging* (Vol. 20, Issue 7, pp. 723–734). Oxford University Press. https://doi.org/10.1093/ehjci/jez094

Ferreira, V. M., Marcelino, M., Piechnik, S. K., Marini, C., Karamitsos, T. D., Ntusi, N. A. B., Francis, J. M., Robson, M. D., Arnold, J. R., Mihai, R., Thomas, J. D. J., Herincs, M., Hassan-Smith, Z. K., Greiser, A., Arlt, W., Korbonits, M., Karavitaki, N., Grossman, A. B., Wass, J. A. H., & Neubauer, S. (2016). *Pheochromocytoma Is Characterized by Catecholamine-Mediated Myocarditis, Focal and Diffuse Myocardial Fibrosis, and Myocardial Dysfunction*.

Ferreira, V. M., Piechnik, S. K., Dall'armellina, E., Karamitsos, T. D., Francis, J. M., Ntusi, N., Holloway, C., Choudhury, R. P., Kardos, A., Robson, M. D., Friedrich, M. G., & Neubauer, S. (n.d.). *T 1 Mapping for the Diagnosis of Acute Myocarditis Using CMR Comparison to T 2-Weighted and Late Gadolinium Enhanced Imaging*.

Ferreira, V. M., Schulz-Menger, J., Holmvang, G., Kramer, C. M., Carbone, I., Sechtem, U., Kindermann, I., Gutberlet, M., Cooper, L. T., Liu, P., & Friedrich, M. G. (2018). Cardiovascular Magnetic Resonance in Nonischemic Myocardial Inflammation: Expert Recommendations. In *Journal of the American College of Cardiology* (Vol. 72, Issue 24, pp. 3158–3176). Elsevier USA. https://doi.org/10.1016/j.jacc.2018.09.072

Fontana, M., Banypersad, S. M., Treibel, T. A., Abdel-Gadir, A., Maestrini, V., Lane, T., Gilbertson, J. A., Hutt, D. F., Lachmann, H. J., Whelan, C. J., Wechalekar, A. D., Herrey, A. S., Gillmore, J. D., Hawkins, P. N., & Moon, J. C. (2015). Differential myocyte responses in patients with cardiac transthyretin amyloidosis and light-chain amyloidosis: A cardiac MR imaging study. *Radiology*, *277*(2). https://doi.org/10.1148/radiol.2015141744

Galderisi, M., Cardim, N., D'Andrea, A., Bruder, O., Cosyns, B., Davin, L., Donal, E., Edvardsen, T., Freitas, A., Habib, G., Kitsiou, A., Plein, S., Petersen, S. E., Popescu, B. A., Schroeder, S., Burgstahler, C., & Lancellotti, P. (2015). Themulti-modality cardiac imaging approach to the Athletés heart: An expert consensus of the European Association of Cardiovascular Imaging. *European Heart Journal Cardiovascular Imaging*, *16*(4), 353-353T. https://doi.org/10.1093/ehjci/jeu323

Gillmore, J. D., Maurer, M. S., Falk, R. H., Merlini, G., Damy, T., Dispenzieri, A., Wechalekar, A. D., Berk, J. L., Quarta, C. C., Grogan, M., Lachmann, H. J., Bokhari, S., Castano, A., Dorbala, S., Johnson, G. B., Glaudemans, A. W. J. M., Rezk, T., Fontana, M., Palladini, G., … Hawkins, P. N. (2016). Nonbiopsy diagnosis of cardiac transthyretin amyloidosis. *Circulation*, *133*(24), 2404–2412. https://doi.org/10.1161/CIRCULATIONAHA.116.021612

Granitz, M., Motloch, L. J., Granitz, C., Meissnitzer, M., Hitzl, W., Hergan, K., & Schlattau, A. (2019). Comparison of native myocardial T1 and T2 mapping at 1.5T and 3T in healthy volunteers: Reference values and clinical implications. *Wiener Klinische Wochenschrift*, *131*(7–8). https://doi.org/10.1007/s00508-018-1411-3

Haaf, P., Garg, P., Messroghli, D. R., Broadbent, D. A., Greenwood, J. P., & Plein, S. (2016). Cardiac T1 Mapping and Extracellular Volume (ECV) in clinical practice: A comprehensive review. In *Journal of Cardiovascular Magnetic Resonance* (Vol. 18, Issue 1). BioMed Central Ltd. https://doi.org/10.1186/s12968-016-0308-4

Kahan, A., & Allanore, Y. (2006). Primary myocardial involvement in systemic sclerosis. *Rheumatology*, *45*(SUPPL. 4). https://doi.org/10.1093/rheumatology/kel312

Kahan, A., Coghlan, G., & McLaughlin, V. (2009). Cardiac complications of systemic sclerosis. In *Rheumatology (Oxford, England): Vol. 48 Suppl 3*. https://doi.org/10.1093/rheumatology/kep110

Karamitsos, T. D., Arvanitaki, A., Karvounis, H., Neubauer, S., & Ferreira, V. M. (2020). Myocardial Tissue Characterization and Fibrosis by Imaging. In *JACC: Cardiovascular Imaging* (Vol. 13, Issue 5, pp. 1221–1234). Elsevier Inc. https://doi.org/10.1016/j.jcmg.2019.06.030

Kawel, N., Nacif, M., Zavodni, A., Jones, J., Liu, S., Sibley, C. T., & Bluemke, D. A. (2012). T1 mapping of the myocardium: Intra-individual assessment of the effect of field strength, cardiac cycle and variation by myocardial region. *Journal of Cardiovascular Magnetic Resonance*, *14*(1). https://doi.org/10.1186/1532-429X-14-27

Kawel-Boehm, N., Maceira, A., Valsangiacomo-Buechel, E. R., Vogel-Claussen, J., Turkbey, E. B., Williams, R., Plein, S., Tee, M., Eng, J., & Bluemke, D. A. (2015). Normal values for cardiovascular magnetic resonance in adults and children. In *Journal of Cardiovascular Magnetic Resonance* (Vol. 17, Issue 1). BioMed Central Ltd. https://doi.org/10.1186/s12968-015-0111-7

Kim, P. K., Hong, Y. J., Im, D. J., Suh, Y. J., Park, C. H., Kim, J. Y., Chang, S., Lee, H. J., Hur, J., Kim, Y. J., & Choi, B. W. (2017). Myocardial T1 and T2 mapping: Techniques and clinical applications. In *Korean Journal of Radiology* (Vol. 18, Issue 1, pp. 113–131). Korean Radiological Society. https://doi.org/10.3348/kjr.2017.18.1.113

Liu, D., Borlotti, A., Viliani, D., Jerosch-Herold, M., Alkhalil, M., de Maria, G. L., Fahrni, G., Dawkins, S., Wijesurendra, R., Francis, J., Ferreira, V., Piechnik, S., Robson, M. D., Banning, A., Choudhury, R., Neubauer, S., Channon, K., Kharbanda, R., & Dall'Armellina, E. (2017). CMR Native T1 Mapping Allows Differentiation of Reversible Versus Irreversible Myocardial Damage in ST-Segment-Elevation Myocardial Infarction: An OxAMI Study (Oxford Acute Myocardial Infarction).

Circulation. Cardiovascular Imaging, *10*(8). https://doi.org/10.1161/CIRCIMAGING.116.005986

Ma, Q., Ma, Y., Yu, T., Sun, Z., & Hou, Y. (2021). Radiomics of non-contrast-enhanced T1 mapping: Diagnostic and predictive performance for myocardial injury in acute ST-segment-elevation myocardial infarction. *Korean Journal of Radiology*, *22*(4), 535–546. https://doi.org/10.3348/kjr.2019.0969

Mavrogeni, S. I., Kitas, G. D., Dimitroulas, T., Sfikakis, P. P., Seo, P., Gabriel, S., Patel, A. R., Gargani, L., Bombardieri, S., Matucci-Cerinic, M., Lombardi, M., Pepe, A., Aletras, A. H., Kolovou, G., Miszalski, T., van Riel, P., Semb, A., Gonzalez-Gay, M. A., Dessein, P., … Lima, J. A. C. (2016). Cardiovascular magnetic resonance in rheumatology: Current status and recommendations for use. In *International Journal of Cardiology* (Vol. 217). https://doi.org/10.1016/j.ijcard.2016.04.158

Mavrogeni, S. I., Schwitter, J., Gargani, L., Pepe, A., Monti, L., Allanore, Y., & Matucci-Cerinic, M. (2017). Cardiovascular magnetic resonance in systemic sclerosis: "Pearls and pitfalls". In *Seminars in Arthritis and Rheumatism* (Vol. 47, Issue 1). https://doi.org/10.1016/j.semarthrit.2017.03.020

Mavrogeni, S., Pepe, A., Nijveldt, R., Ntusi, N., Sierra-Galan, L. M., Bratis, K., Wei, J., Mukherjee, M., Markousis-Mavrogenis, G., Gargani, L., Sade, L. E., Ajmone-Marsan, N., Seferovic, P., Donal, E., Nurmohamed, M., Cerinic, M. M., Sfikakis, P., Kitas, G., Schwitter, J., … Cosyns, B. (2022). Cardiovascular magnetic resonance in autoimmune rheumatic diseases: a clinical consensus document by the European Association of Cardiovascular Imaging. *European Heart Journal Cardiovascular Imaging*, *23*(9), E308–E322. https://doi.org/10.1093/ehjci/jeac134

Meloni, A., Maggio, A., Positano, V., Leto, F., Angelini, A., Putti, M. C., Maresi, E., Pucci, A., Basso, C., Marra, M. P., Pistoia, L., de Marchi, D., & Pepe, A. (2020). CMR for myocardial iron overload quantification: calibration curve from the MIOT Network. *European Radiology*, *30*(6). https://doi.org/10.1007/s00330-020-06668-1

Meloni, A., Martini, N., Positano, V., D'Angelo, G., Barison, A., Todiere, G., Grigoratos, C., Barra, V., Pistoia, L., Gargani, L., Ripoli, A., & Pepe, A. (2021). Myocardial T1 Values at 1.5 T: Normal Values for General Electric Scanners and Sex-Related Differences. *Journal of Magnetic Resonance Imaging*, *54*(5). https://doi.org/10.1002/jmri.27639

Meloni, A., Martini, N., Positano, V., de Luca, A., Pistoia, L., Sbragi, S., Spasiano, A., Casini, T., Bitti, P. P., Allò, M., Sanna, P. M. G., de Caterina, R., Sinagra, G., & Pepe, A. (2021). Myocardial iron overload by cardiovascular magnetic resonance native segmental T1 mapping: a sensitive approach that correlates with cardiac complications. *Journal of Cardiovascular Magnetic Resonance*, *23*(1). https://doi.org/10.1186/s12968-021-00765-w

Meloni, A., Pistoia, L., Positano, V., de Luca, A., Martini, N., Spasiano, A., Fotzi, I., Bitti, P. P., Visceglie, D., Alberini, G., Sinagra, G., Pepe, A., & Cademartiri, F. (2022). Increased myocardial extracellular volume is associated with myocardial iron overload and heart failure in thalassemia major. *European Radiology*. https://doi.org/10.1007/s00330-022-09120-8

Messroghli, D. R., Moon, J. C., Ferreira, V. M., Grosse-Wortmann, L., He, T., Kellman, P., Mascherbauer, J., Nezafat, R., Salerno, M., Schelbert, E. B., Taylor, A. J., Thompson,

R., Ugander, M., van Heeswijk, R. B., & Friedrich, M. G. (2017). Clinical recommendations for cardiovascular magnetic resonance mapping of T1, T2, T2 and extracellular volume: A consensus statement by the Society for Cardiovascular Magnetic Resonance (SCMR) endorsed by the European Association for Cardiovascular Imaging (EACVI). In *Journal of Cardiovascular Magnetic Resonance* (Vol. 19, Issue 1). https://doi.org/10.1186/s12968-017-0389-8

Messroghli, D. R., Radjenovic, A., Kozerke, S., Higgins, D. M., Sivananthan, M. U., & Ridgway, J. P. (2004). Modified look-locker inversion recovery (MOLLI) for high-resolution T 1 mapping of the heart. *Magnetic Resonance in Medicine*, *52*(1), 141–146. https://doi.org/10.1002/mrm.20110

Messroghli, D. R., Walters, K., Plein, S., Sparrow, P., Friedrich, M. G., Ridgway, J. P., & Sivananthan, M. U. (2007). Myocardial T1 mapping: Application to patients with acute and chronic myocardial infarction. *Magnetic Resonance in Medicine*, *58*(1), 34–40. https://doi.org/10.1002/mrm.21272

Mordi, I., Carrick, D., Bezerra, H., & Tzemos, N. (2016). T1 and T2 mapping for early diagnosis of dilated non-ischaemic cardiomyopathy in middle-aged patients and differentiation from normal physiological adaptation. *European Heart Journal Cardiovascular Imaging*, *17*(7), 797–803. https://doi.org/10.1093/ehjci/jev216

Nie, L. Y., Wang, X. D., Zhang, T., & Xue, J. (2019). Cardiac complications in systemic sclerosis: Early diagnosis and treatment. In *Chinese Medical Journal* (Vol. 132, Issue 23, pp. 2865–2871). Lippincott Williams and Wilkins. https://doi.org/10.1097/CM9.0000000000000535

Ntusi, N. A., Piechnik, S. K., Francis, J. M., Ferreira, V. M., Rai, A. B., Matthews, P. M., Robson, M. D., Moon, J., Wordsworth, P. B., Neubauer, S., & Karamitsos, T. D. (2014). Subclinical myocardial inflammation and diffuse fibrosis are common in systemic sclerosis - A clinical study using myocardial T1-mapping and extracellular volume quantification. *Journal of Cardiovascular Magnetic Resonance*, *16*(1). https://doi.org/10.1186/1532-429X-16-21

Ntusi, N., O'Dwyer, E., Dorrell, L., Wainwright, E., Piechnik, S., Clutton, G., Hancock, G., Ferreira, V., Cox, P., Badri, M., Karamitsos, T., Emmanuel, S., Clarke, K., Neubauer, S., & Holloway, C. (2016). HIV-1-Related Cardiovascular Disease Is Associated with Chronic Inflammation, Frequent Pericardial Effusions, and Probable Myocardial Edema. *Circulation: Cardiovascular Imaging*, *9*(3). https://doi.org/10.1161/CIRCIMAGING.115.004430

Pennell, D. J., Udelson, J. E., Arai, A. E., Bozkurt, B., Cohen, A. R., Galanello, R., Hoffman, T. M., Kiernan, M. S., Lerakis, S., Piga, A., Porter, J. B., Walker, J. M., & Wood, J. (2013). Cardiovascular function and treatment in β-thalassemia major: A consensus statement from the american heart association. *Circulation*, *128*(3). https://doi.org/10.1161/CIR.0b013e31829b2be6

Pepe, A., Meloni, A., Filosa, A., Pistoia, L., Borsellino, Z., D'Ascola, D. G., Lisi, R., Putti, M. C., Allò, M., Gamberini, M. R., Quarta, A., Fidone, C., Casini, T., Restaino, G., Midiri, M., Mangione, M., Positano, V., & Casale, M. (2020). Prospective CMR Survey in Children With Thalassemia Major: Insights From a National Network. In *JACC:*

Cardiovascular Imaging (Vol. 13, Issue 5, pp. 1284–1286). Elsevier Inc. https://doi.org/10.1016/j.jcmg.2019.12.015

Pepe, A., Meloni, A., Pistoia, L., Cuccia, L., Gamberini, M. R., Lisi, R., D'Ascola, D. G., Rosso, R., Allò, M., Spasiano, A., Restaino, G., Righi, R., Mangione, M., Positano, V., & Ricchi, P. (2018). MRI multicentre prospective survey in thalassaemia major patients treated with deferasirox versus deferiprone and desferrioxamine. *British Journal of Haematology*, *183*(5), 783–795. https://doi.org/10.1111/bjh.15595

Pepe, A., Pistoia, L., Gamberini, M. R., Cuccia, L., Lisi, R., Cecinati, V., Maggio, A., Sorrentino, F., Filosa, A., Rosso, R., Messina, G., Missere, M., Righi, R., Renne, S., Vallone, A., Dalmiani, S., Positano, V., Midiri, M., & Meloni, A. (2022). National networking in rare diseases and reduction of cardiac burden in thalassemia major. *European Heart Journal*, *43*(26), 2482–2492. https://doi.org/10.1093/eurheartj/ehab851

Piechnik, S. K., Ferreira, V. M., Dall'Armellina, E., Cochlin, L. E., Greiser, A., Neubauer, S., & Robson, M. D. (2010). Shortened Modified Look-Locker Inversion recovery (ShMOLLI) for clinical myocardial T1-mapping at 1.5 and 3 T within a 9 heartbeat breathhold. *Journal of Cardiovascular Magnetic Resonance*, *12*(1). https://doi.org/10.1186/1532-429X-12-69

Plein, S., Greenwood, J., & Ridgway, J. P. (2011). Cardiovascular MR Manual. In *Cardiovascular MR Manual*. https://doi.org/10.1007/978-1-84996-362-6

Poindron, V., Chatelus, E., Canuet, M., Gottenberg, J. E., Arnaud, L., Gangi, A., Gavand, P. E., Guffroy, A., Korganow, A. S., Germain, P., Sibilia, J., el Ghannudi, S., & Martin, T. (2020). T1 mapping cardiac magnetic resonance imaging frequently detects subclinical diffuse myocardial fibrosis in systemic sclerosis patients. *Seminars in Arthritis and Rheumatism*, *50*(1), 128–134. https://doi.org/10.1016/j.semarthrit.2019.06.013

Ponsiglione, A., Gambardella, M., Green, R., Cantoni, V., Nappi, C., Ascione, R., de Giorgi, M., Cuocolo, R., Pisani, A., Petretta, M., Cuocolo, A., & Imbriaco, M. (2022). Cardiovascular magnetic resonance native T1 mapping in Anderson-Fabry disease: a systematic review and meta-analysis. In *Journal of Cardiovascular Magnetic Resonance* (Vol. 24, Issue 1). BioMed Central Ltd. https://doi.org/10.1186/s12968-022-00859-z

Popescu, I. A., Werys, K., Zhang, Q., Puchta, H., Hann, E., Lukaschuk, E., Ferreira, V. M., & Piechnik, S. K. (2021). Standardization of T1-mapping in cardiovascular magnetic resonance using clustered structuring for benchmarking normal ranges. *International Journal of Cardiology*, *326*, 220–225. https://doi.org/10.1016/j.ijcard.2020.10.041

Ramazzotti, A., Pepe, A., Positano, V., Rossi, G., de Marchi, D., Brizi, M. G., Luciani, A., Midiri, M., Sallustio, G., Valeri, G., Caruso, V., Centra, M., Cianciulli, P., de Sanctis, V., Maggio, A., & Lombardi, M. (2009). Multicenter validation of the magnetic resonance T2* technique for segmental and global quantification of myocardial iron. *Journal of Magnetic Resonance Imaging*, *30*(1), 62–68. https://doi.org/10.1002/jmri.21781

Rauhalammi, S. M. O., Mangion, K., Barrientos, P. H., Carrick, D. J. A., Clerfond, G., McClure, J., McComb, C., Radjenovic, A., & Berry, C. (2016). Native myocardial longitudinal (T1) relaxation time: Regional, age, and sex associations in the healthy adult heart. *Journal of Magnetic Resonance Imaging*, *44*(3), 541–548. https://doi.org/10.1002/jmri.25217

Regitz-Zagrosek, V. (2006). Therapeutic implications of the gender-specific aspects of cardiovascular disease. In *Nature Reviews Drug Discovery* (Vol. 5, Issue 5, pp. 425–439). https://doi.org/10.1038/nrd2032

Reiter, U., Reiter, G., Dorr, K., Greiser, A., Maderthaner, R., & Fuchsjäger, M. (2014). Normal diastolic and systolic myocardial T1 values at 1.5-T MR imaging: Correlations and blood normalization. *Radiology*, *271*(2). https://doi.org/10.1148/radiol.13131225

Rodríguez-Reyna, T. S., Morelos-Guzman, M., Hernández-Reyes, P., Montero-Duarte, K., Martínez-Reyes, C., Reyes-Utrera, C., Madrid, J. V. la, Morales-Blanhir, J., Núñez-Álvarez, C., & Cabiedes-Contreras, J. (2014). Assessment of myocardial fibrosis and microvascular damage in systemic sclerosis by magnetic resonance imaging and coronary angiotomography. *Rheumatology (United Kingdom)*, *54*(4), 647–654. https://doi.org/10.1093/rheumatology/keu350

Rosmini, S., Bulluck, H., Captur, G., Treibel, T. A., Abdel-Gadir, A., Bhuva, A. N., Culotta, V., Merghani, A., Fontana, M., Maestrini, V., Herrey, A. S., Chow, K., Thompson, R. B., Piechnik, S. K., Kellman, P., Manisty, C., & Moon, J. C. (2018). Myocardial native T1 and extracellular volume with healthy ageing and gender. *European Heart Journal Cardiovascular Imaging*, *19*(6). https://doi.org/10.1093/ehjci/jey034

Shanbhag, S. M., Chen, M. Y., Bandettini, W. P., Kellman, P., Xue, H., Zuehlsdorff, S., Glielmi, C., Guehring, J., Hsu, L.-Y., & Arai, A. E. (2011). Image quality and diagnostic accuracy of inline motion-corrected (moco) first-pass stress myocardial perfusion images. *Journal of Cardiovascular Magnetic Resonance*, *13*(S1). https://doi.org/10.1186/1532-429x-13-s1-o12

Swoboda, P. P., McDiarmid, A. K., Erhayiem, B., Broadbent, D. A., Dobson, L. E., Garg, P., Ferguson, C., Page, S. P., Greenwood, J. P., & Plein, S. (2016). Assessing Myocardial Extracellular Volume by T1 Mapping to Distinguish Hypertrophic Cardiomyopathy from Athlete's Heart. In *Journal of the American College of Cardiology* (Vol. 67, Issue 18, pp. 2189–2190). Elsevier USA. https://doi.org/10.1016/j.jacc.2016.02.054

Tessa, C., Diciotti, S., Landini, N., Lilli, A., del Meglio, J., Salvatori, L., Giannelli, M., Greiser, A., Vignali, C., & Casolo, G. (2015). Myocardial T1 and T2 mapping in diastolic and systolic phase. *International Journal of Cardiovascular Imaging*, *31*(5), 1001–1010. https://doi.org/10.1007/s10554-015-0639-5

Thompson, R. B., Chow, K., Khan, A., Chan, A., Shanks, M., Paterson, I., & Oudit, G. Y. (2013). T1 mapping with cardiovascular MRI is highly sensitive for fabry disease independent of hypertrophy and sex. *Circulation: Cardiovascular Imaging*, *6*(5), 637–645. https://doi.org/10.1161/CIRCIMAGING.113.000482

Wu, E. X., Tang, H., Wong, K. K., & Wang, J. (2004). Mapping Cyclic Change of Regional Myocardial Blood Volume Using Steady-State Susceptibility Effect of Iron Oxide

Nanoparticles. *Journal of Magnetic Resonance Imaging*, *19*(1), 50–58. https://doi.org/10.1002/jmri.10426

ACKNOWLEDGMENTS

I would particularly like to thank all the healthy volunteers who took part in the study, generously giving their time for free and undergoing the cardiac MRI examination, which enabled us to obtain normal T1 values for the MR scanner at the Institute of Radiology of the University of Padua.

Their contribution will allow the correct use of T1 mapping for quantitative characterisation of the myocardium, promoting earlier diagnosis and better clinical management of patients with cardiological pathology.

I would also like to thank all the employees of the Institute of Radiology, University of Padua.